Effects of Projected Twenty-First Century Sea Level Rise, Storm Surge, and River Flooding on Water Levels in Puget Sound Floodplains and Estuaries

Joseph J. Hamman

A thesis
Submitted in partial fulfillment of the
requirements for the degree of

Master of Science in Civil Engineering

University of Washington

2012

Committee:

Alan F. Hamlet

Erkan Istanbulluoglu

Program Authorized to Offer Degree:

Civil and Environmental Engineering

University of Washington

Abstract

Effects of Projected Twenty-First Century Sea Level Rise, Storm Surge, and River Flooding on Water Levels in Puget Sound Floodplains and Estuaries

Joseph J. Hamman

Chair of the Supervisory Committee:

Professor Alan F. Hamlet

Department of Civil and Environmental Engineering

Near coastal environments have been identified as some of the most likely to be impacted by climate change. Observed changes in Puget Sound sea level and flood magnitudes are in line with those projected by previous climate change impacts studies. Current understanding of the combined effects of these changes is relatively low and has prompted us to explore the ways in which their co-occurrence will influence near coastal ecosystems and infrastructure. This project examines the effects of climate change on the lower reaches of Puget Sound rivers by investigating changes in storm surge, sea level rise, and riverine flooding. The project utilizes numerical models to quantify the shifts in hydraulic conditions expected in the Skagit and Nisqually river basins. Global climate model simulations from the ECHAM-5 climate model were used as the climate forcings and were 1) statistically downscaled using the hybrid delta method, and 2) dynamically downscaled using the WRF regional climate model. Naturalized flows produced using the Variable Infiltration Capacity hydrology model were used to drive reservoir models that simulate flood control operations. Storm surge was calculated using a regression approach that included anomalous atmospherics forcings simulated by the WRF model. A 2D hydrodynamic model was used to estimate water surface elevations in the Skagit and Nisqually River estuaries using resampled hourly hydrographs keyed to regulated daily flood flows produced by a daily time step reservoir simulation model and tide predictions adjusted for SLR and storm surge. Combining peak annual storm surge with expected sea level rise, the historic (1970-1999) 100-yr peak tidal anomaly is found to be exceeded every year by the 2020s. By the 2050s, the extrapolated 100-yr riverine flood events are found to increase by 30% and 25% in the Skagit and Nisqually Rivers, respectively. In the Skagit River, the combined effect of sea level rise and larger floods yields increased areal flood inundation up to 80% relative to the present “100-year” flood.

ACKNOWLEDGMENTS

This research was funded by the Nature Conservancy (TNC) and the Environmental Protection Agency (EPA) under cooperative agreement no. EPA-R10-PS-1004. I would like to thank my advisor, Professor Alan. F. Hamlet, for his insightful direction and guidance throughout this project. This project would not have been possible without the assistance and previous work completed by Se-Yuen Lee, Matt Stumbaugh, and Professor Eric P. Salathé. The support of my friends and colleagues in the Department of Civil and Environmental Engineering contributed to the success of this project. Finally, I am perpetually grateful for the unending support of by wife Lauren and her enduring support of my academic ventures.

TABLE OF CONTENTS

List of Figures

List of Tables

Glossary

CDF	Cumulative Density Function
CMIP3	Coupled Model Intercomparison Project
CRBCCS	Columbia River Basin Climate Change Study
ENSO	El Niño Southern Oscillation
EOF	Empirical Orthogonal Function
FEMA	Federal Emergency Management Agency
FERC	Federal Energy Regulatory Commission
GCM	Global Climate Model
IPCC	International Panel on Climate Change
NOAA	National Oceanic and Atmospheric Administration
PC	Principle Component
PDO	Pacific Decal Oscillation
PNW	Pacific Northwest
PSE	Puget Sound Energy
RCM	Regional Climate Model
SCL	Seattle City Light
SRCSR	Skagit River Climate Science Report
SRES	Special Report on Emission Scenarios
SST	Sea Surface Temperature
SVD	Singular Value Decomposition
TP	Tacoma Power
USACE	United States Army Corps of Engineers
USGS	United States Geologic Survey
VIC	Variable Infiltration Capacity Model
WRF	Weather Research Forecasting

1 Introduction

There is strong scientific consensus that human behavior is altering the global climate system via greenhouse gas emissions. The projected changes in climate resulting from increases in greenhouse gas concentrations will substantially impact human and natural systems in the twenty-first century (IPCC, 2007). Since the industrial revolution, greenhouse gas concentrations have increased by approximately 36% (IPCC, 2007), resulting in increased mean global surface temperatures of 0.74°C (IPCC, 2007). Extensive effort in recent years by the climate science community has been focused on developing projections of the future climate. These projections consider changes in population, greenhouse gas emissions, dynamic climate feedbacks, radiative forcings, etc. While the results of the numerous global climate model (GCM) simulations based on a range of emission scenarios vary considerably, there is wide scientific agreement on the basic direction and magnitude of future climate changes, particularly for temperature impacts (IPCC, 2007).

Observed changes in the climate of the Pacific Northwest (PNW) exceed the global changes described above. Annually averaged temperature and precipitation for the twentieth century were found to increase 0.7-0.9°C and 13%-38%, respectively (Mote, 2003). These changes alone have had noticeable impacts on streamflow timing (Stewart, et al., 2005), snowpack (Hamlet, et al., 2005; Mote et al., 2005), melting glaciers (IPCC, 2007; Lee & Hamlet, 2007), ecosystem function (McKenzie, et al., 2004; Littell, et al., 2009; Mantua, et al., 2010), and the onset of spring (Cayan, et al., 2001). In response to warming and the subsequent loss of terrestrial ice, global and regional sea levels have risen, and are projected to continue to rise (Church, et al., 2004; Church & White, 2006;

IPCC, 2007; Mote, et al., 2008; Nicholls & Cazenave, 2010). Natural variability also greatly influences PNW climate. The Pacific Decadal Oscillation (PDO) (Mantua et al., 1997; Mantua & Hare, 2002) and El Niño Southern Oscillation (ENSO) are two climate phenomena that have strong effects on seasonal temperature (UW CIG), precipitation (UW CIG), flood risk (Hamlet & Lettenmaier, 2007), and sea level (figure 10A) in the PNW.

Figure 1 - Location of the Skagit and Nisqually River Basins. The Skagit and Nisqually rivers drain approximately 2656 and 517 sq. mi. respectively. Both rivers have headwaters in the Cascade Mountains and drain into the Puget Sound.

Water levels in estuaries are particularly sensitive to climate change. These areas are impacted from the marine side by storm surge and sea level rise (SLR), and from the freshwater side by seasonal changes in river flow and hydrologic extremes. This study quantifies future lowland water levels caused by projected impacts on sea-level rise, storm surge, and riverine flooding in the Skagit and Nisqually River Basins, located in the Puget Sound Region of Washington State. Coincident storm surge and riverine

flooding are evaluated using statistical and physically modeling techniques. A principal goal of this research is to develop tools and approaches to make climate change projections that are useful for future planning in coastal areas.

In this study the time series behavior of individual storms, simulated by a regional climate model, is kept intact within the storm surge and hydrology models. In this way, coincident storm surge and riverine flooding can be modeled as products of each individual storm. This practice distinguishes this study from other recent climate change impacts studies. Storms are the variable drivers of the highest estuarine water levels both because of the barometric and wind effects on sea levels, and because of the freshwater floods that they generate (Cayan, et al., 2008). This temporal consistency in the modeling facilitates the realistic pairing of storm surge and river flooding events in the projection of impacts to estuarine flooding. Furthermore, maintaining this temporal consistency allows for the review of all aspects of individual storm events, including precipitation, flooding, wind and pressure patterns.

The research described here has immediate implications for coastal and riverine floodplain management. Nearly all present-day floodplain management strategies rely entirely on the historical record, which is a questionable practice in a non-stationary climate (Milly, et al., 2008). Using scenario-based approaches to manage floodplain environments, such as the one demonstrated in this paper, may ultimately inform solutions to the problems created by a changing climate.

Section 2 of this paper outlines the origins of the observed data used for this project. Section 3 describes the methods used to determine storm surge, sea level and

riverine flooding. Section 3 also discusses the numerical models used including those used and developed by contributing projects. Finally, Section 4 discusses the results of this study, initially one variable at a time, then using a combined approach that assesses their coincident occurrence and utilizes hydrodynamic modeling.

2 Data

2.1 Tidal Data

Observed hourly tidal data for Seattle, Sneeoosh Point, and Yoman Point were obtained from the National Oceanic and Atmospheric Administration's (NOAA) tide station network database (http://tidesandcurrents.noaa.gov/). This data was previously corrected for any sensor error but was not adjusted to remove storm surge anomalies brought on by atmospheric forcings. The separation of these two signals will be described in section 3.6.

Following the methodology used by the Federal Emergency Management Agency (FEMA) for the Skagit County Flood Insurance Study, the Seattle tidal time series was used as the historic observations for both the Skagit and Nisqually rivers. While the observed time series do not match perfectly, the significantly longer period of record at the Seattle station and the geographic proximity of the study locations to Seattle justify the substitution.

Table 1 – NOAA tide gauges used for this project. Sneeoosh Point and Yoman Point were the two closest tide gauges to the studied estuaries. Neither contained a long enough period of record to facilitate their use in the regression model.

Station Name	Station ID	Begin Date	End Date
Seattle, Puget Sound, WA	9447130	1899-01-01	2012-03-28
Sneeoosh Point, WA	9448576	2000-05-05	2000-08-19
Yoman Point, Anderson Island, WA	9446828	1996-03-09	1996-11-12

2.2 River Flows

Mean daily flows for the Skagit and Nisqually Rivers were obtained from the United States Geologic Survey (USGS) website (waterdata.usgs.gov/nwis). Hourly flows for the Skagit River at Mt. Vernon were used to disaggregate daily flood hydrographs. All USGS flows used for this project were reviewed for quality control prior to their publishing. No further data processing was deemed necessary.

Observed flows for the Skagit River at the Concrete, Mt. Vernon and Sauk stations were obtained from USGS. For the Nisqually River, USGS flows at La Grande, McKenna and the Centralia Diversion Canal were used. The Centralia hydropower diversion (via the Centralia Diversion Canal) in the Nisqually system does not include a storage component that would influence flood flows, and was therefore not modeled in either the reservoir or hydrodynamic models. Because travel times within the diversion are much less than the daily timestep of the model, these two stations were combined to create a semi-naturalized flow at McKenna.

Table 2 - USGS flows used for this project. Daily flows were used in the bias correction of raw VIC flow and in the calibration of the reservoir models. Hourly flows for the Skagit River at Mt. Vernon and Nisqually River at McKenna were used to disaggregate daily flows for use in the hydrodynamic models.

Station Name	Station Number	Begin Date	End Date
Skagit River at Concrete, WA	12194000	1924-10-01	2012-03-28
Skagit River at Mt. Vernon, WA[1]	12199000	1908-05-01	2012-03-28
Nisqually River at La Grande, WA	12086500	1906-10-01	2012-03-28
Sauk River near Sauk, WA	12189500	1911-04-01	2012-03-28
Centralia Power Canal near McKenna, WA	12089208	1979-03-21	2012-03-28
Nisqually River at McKenna, WA	12089500	1947-10-01	2012-03-28

2.3 Reservoir Operations

Puget Sound Energy (PSE), Seattle City Light (SCL) and the United State Army Corps of Civil Engineers (USACE) provided daily reservoir levels for the Skagit River. Tacoma Power (TP) and USGS provided daily reservoir levels for the Nisqually River. Operational constraints, such as reservoir design, and flood operation rule curves were obtained from the USACE for the Skagit River reservoirs and through personal communications with TP personnel for the Nisqually River reservoirs. Minimum flow requirements were outlined for each hydropower project in their respective Federal Energy Regulatory Commission (FERC) license.

2.4 Sea Surface Temperatures and Climate Indices

Historic Monthly values for the Niño 3.4 index were obtained from the NOAA's Climate Prediction Center (http://www.cpc.ncep.noaa.gov/data/indices). The indices

[1] Hourly flow record is from 1988-10-01 to 2007-09-30.

were calculated using the OISST.v3 gridded Sea Surface Temperature Data Set (Smith, et al., 2008) between (5°N-5°S, 170°W -120°W) with a climatological base period of 1981-2010.

3 Methods

The project uses a sequence of physically and empirically based and numerical models to quantify the shifts in hydraulic conditions expected in the Skagit and Nisqually River Basins (Figure 2). The results of the ECHAM-5 climate model were used as the future climate forcings and were dynamically downscaled using Weather Research Forecast (WRF) regional climate model (RCM). Statistically downscaled results from previous studies using the Hybrid Delta approach (Hamlet et al. 2010) were also used as a point of comparison. Downscaled and bias-corrected outputs from the WRF simulations were used as the atmospheric inputs for the Variable Infiltration Capacity (VIC) distributed hydrology model and a linear regression storm surge model. Daily streamflows from the VIC simulations were used to force reservoir operation models for both river systems. The final step was to input disaggregated hourly flows and tides to a hydrodynamic model to determine the depth and spatial extent of inundation during flooding.

This section outlines the methods used in developing temporally consistent projections of streamflow and storm surge. A schematic detailing the chain of numerical models used for this project is shown in figure 2. Some of the subsections herein are descriptions of methods used by others in preparing input data used for this project. Although those sections describe work not completed during this project, they are included for continuity and clarity of process.

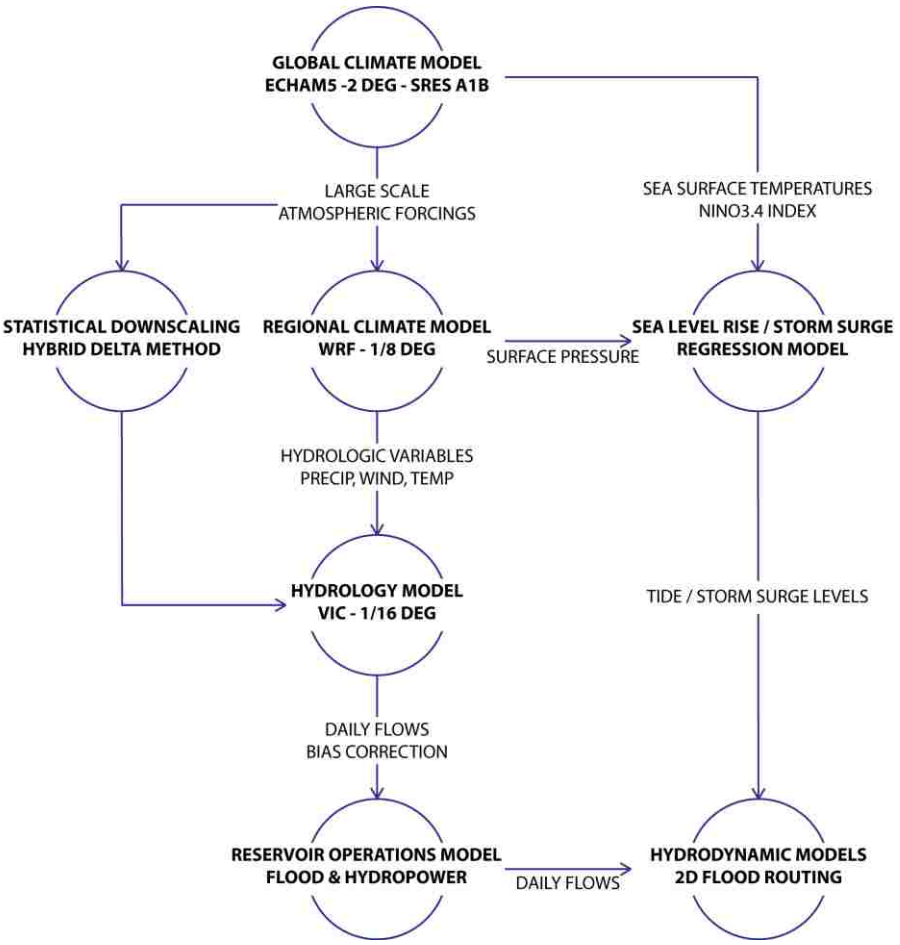

Figure 2 - Flow chart demonstrating the chain of numerical models used for this project. Temporal consistency is maintained throughout, according to the time behavior set by the GCM or observations. In this way, the floods modeled using the hydrodynamic model were representative of the complete atmospheric condition that created both the storm surge and river flooding.

3.1 Climate Models

Climate models simulate coupled atmospheric and ocean physics and are used here to project the future climate at both the global and regional scale given scenarios of changing greenhouse gas forcing. In recent years, significant research has been devoted to the development of GCMs capable of resolving the impact of increased greenhouse gas concentrations, widespread land use change, variable solar inputs, and dynamic climate feedbacks, etc. A thorough discussion of the development, model physics, operation, and results of modern climate models can be found in the 4th IPCC report (IPCC, 2007)

Figure 3 shows the model simulated climate for the 20th and 21st century for the PNW (Mote & Salathe, 2010). Projecting into the future, the 21 GCMs presented in the IPCC AR4 report show an average increase in annual temperature of 1.1°C by the 2020s, 1.8°C by the 2040s and 3.0°C by the 2080s compared to average temperatures from 1970 to 1999. While annual precipitation changes, averaged over all models, are less significant (+1% to +2%), the majority of the models indicate intensification of the current seasonal precipitation cycle (wet winters and dry summers) in response to increased greenhouse forcing (Mote & Salathe, 2010). Such changes have important implications for flooding in western WA, which typically experiences peak annual flows in early winter, when precipitation is projected to increase.

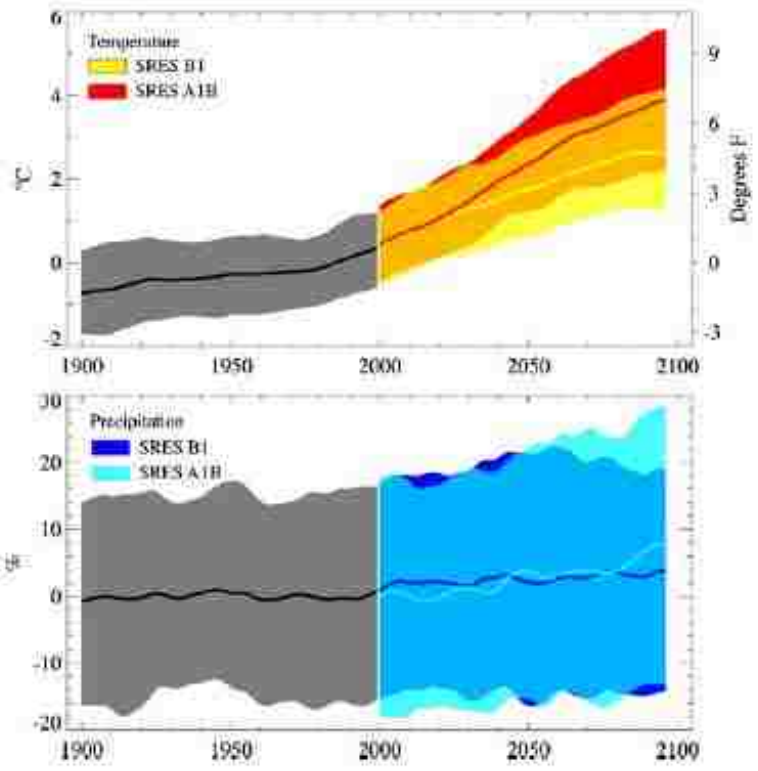

Figure 3 – Projections of annual temperature (top) and precipitation (bottom) for the 20th and 21st century for the PNW, relative to the 1970-1999 mean. The heavy smooth curve for each scenario is the REA value, calculated for each year and then smoothed using loess. Source: Mote & Salathé (2010).

There are many different GCMs and downscaling techniques available for use in climate impact studies. For this project the CMIP3 results from ECHAM-5 model, A1B emissions scenario, ensemble member one, were used as the building blocks for subsequent models and techniques. This model is the fifth generation atmosphere general circulation model developed at the Max Plank Institute for Meteorology. The EHCAM-5 model is coupled to the MPI-OM ocean model, also developed at the Max Plank Institute for Meteorology. The model was run at T63 spatial resolution (approximately 2°×2° or 140km x 210km at mid-latitudes). Model output was six hours, which was also used as the forcing interval for the RCM.

In their evaluation of 10 climate models, Salathé, et al. (2007) concluded that the ECHAM-5 most accurately simulates the observed climate in the PNW relative to the other models. The model also ranked highly using updated criteria established by Mote & Salathé (2010). Considering temperature and precipitation as primary variables, both studies found the ECHAM-5 to show small biases relative to reanalysis. The PNW temperature and precipitation changes predicted by the ECHAM-5 model also fall near the averages of the other GCMs. Lastly, among the twenty-one coupled GCMs included in the IPCC AR4 report, the ECHAM-5/MPI-OM was the only model to replicate the observed variability of the ENSO pattern in the equatorial Pacific sea surface temperatures (Lin, 2007), an important driver of interannual climate variability in the PNW. These qualities make the ECHAM-5 a good selection for single-model consideration.

The A1B emissions scenario was outlined in the fourth IPCC report. Its storyline includes a future world of rapid economic growth and population that peaks by the

middle of the twenty-first century. This scenario includes rapid introduction of new technologies and increased connectivity between regions. In the A1B world, the approach to developing new technologies is balance between fossil fuel and non-fossil fuel energy sources. This scenario represents a "business as usual" progression of policy, economy, and technological development until the mid-twenty-first century, followed by more substantial greenhouse gas mitigation in the second half of the century (IPCC, 2007).

Due to the low spatial and temporal resolution of GCMs, simulations of regional and local scale climates have many shortcomings, especially in topographically complex regions, such as the PNW. Mass, et al. (2003) show that a grid resolution of 15 km or less is necessary to successfully resolve the orographic precipitation in the PNW. Thus in order to use contemporary GCM results for regional and local applications some form of downscaling and bias correction must be employed. Downscaling refers to the process of relating large-scale climate features (simulated by GCMs) to finer scale effects. In general, there are two basic approaches used to downscale GCM results, statistical (section 3.2) and dynamic (section 3.3); both methods are used in this study.

3.2 Statistical Downscaling Approach – Hybrid Delta Method

Hydrologic simulations using the Hybrid Delta statistical downscaling method (Hamlet, et al., 2010) are used as a point of comparison in this study. Using bias-corrected and spatially disaggregated (Wood, et al., 2002) monthly climate projections from a GCM for each $1/16^{th}$ degree grid cell, monthly values are assigned a plotting position. Monthly observations (1916-2006) are then remapped onto the bias-corrected

GCM data (figure 4), producing a set of transformed observations that mimic the projected future conditions at a monthly time step. The observed daily time series for each historic month is then adjusted to fit the remapped value to produce a daily time series for the future conditions. This process is repeated for all grid cells in the domain. This method produces realistic storms, and projections of hydrologic extremes, based on observed patterns from the historical record. However, potential changes in the probability distributions of daily precipitation, seasonality, storm size, storm track, and interarrival time of storms may not captured by this approach.

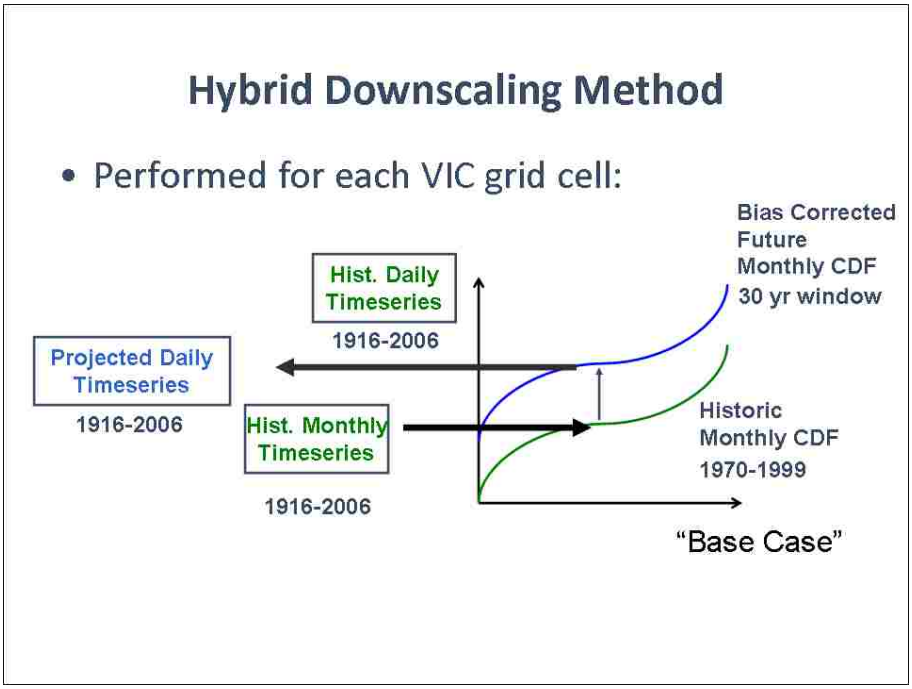

Figure 4 - Schematic diagram of the final data processing steps for the hybrid delta downscaling method. Source: Hamlet et al. (2010).

3.3 Dynamic Downscaling – Regional Climate Model

The dynamic downscaling technique used in this study utilized the WRF regional climate model implemented over the PNW at 12km resolution. This model was forced at the outer boundary by the NCAR Reanalysis (1950-2010) for the historical run and the

ECHAM-5 GCM (1970-1999, 2010-2039, and 2040-2069) for the A1B emissions scenario. The RCM was forced to meet the exterior boundary conditions set by the large-scale climate forcings and "nudged" internally to partially preserve the overall atmospheric structure prescribed by reanalysis or the GCM (Salathé, et al., 2010; Salathé, et al., 2012).

In the context of understanding future hydrologic extremes, the use of a dynamic downscaling approach better represents fine scale topography, such as the Cascade Mountains, and atmospheric processes such as orographic precipitation that are crucial to understanding climate change impacts in Western Washington. When forced by reanalysis data, the model successfully captures important storm characteristics related to flooding (figure 5). The outputs of the RCM were bias-corrected at a daily timestep using a similar approach to the one described in section 3.2, but with different objectives. The two bias-correction procedures differ in that WRF output was bias corrected at a daily timestep while the hybrid-delta method was performed at a monthly timestep. Furthermore, this revised method maintains the explicit character of storms simulated by the RCM (e.g. seasonality, location, size, intensity, interarrival time, etc.) by directly preserving the spatial and temporal patterns of the WRF output. For further information on the methods involved in the WRF-regional climate model study see Salathé, et al. (2012).

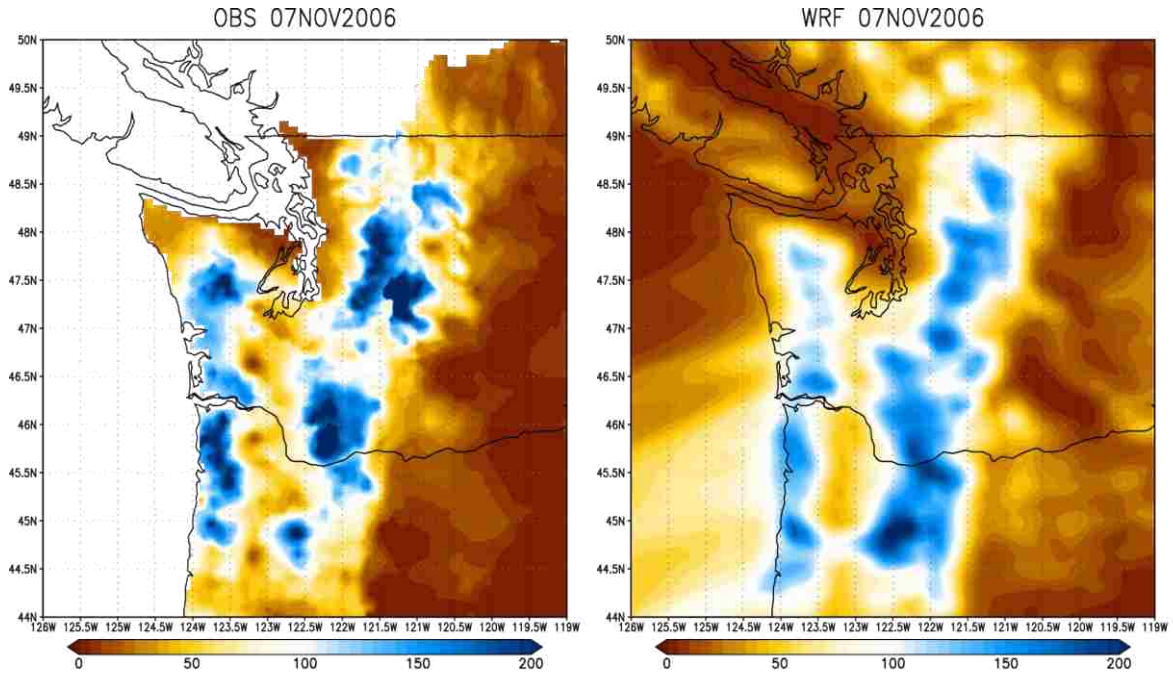

Figure 5 - Example of the WRF regional climate model compared to observations for the Nov. 7, 2006 storm. Dynamic downscaling provides much higher resolution relative to the resolution provided by the GCMs. Rather than depending on the historical spatial patterns, the RCM explicitly determines fine scale weather as would occur given the large scale atmospheric patters of the GCM. Source: Hamlet et al., 2011 (conference presentation).

3.4 Hydrologic Modeling

The hydrologic model used to produce daily streamflows for this project was the Variable Infiltration Capacity (VIC) model (Liang, et al., 1994; Liang, et al., 1996; Nijssen, et al., 1997; Gao, et al., 2010). The VIC model has been applied extensively to study climate change impacts at regional scales (Lee et al., 2009; Elsner, et al., 2010; Hamlet, et al., 2010; Vano, et al., 2010). VIC is a distributed hydrology model that solves the energy and water balance equations at each grid cell. Inputs into the model are daily maximum and minimum temperature, wind, and precipitation in addition to fixed topography and land cover characteristics. Hybrid-Delta VIC simulations were extracted from the CBCCSP archives (Hamlet, et al., 2010) and Skagit 2060 project (Lee & Hamlet, 2011). ECHAM5/WRF/VIC simulations were extracted from the archives of

Salathé et al. (2012). For this project, additional calibration of the routing model was carried out to improve realizations of daily hydrologic extremes in the Skagit and Nisqually Basins. Monthly simulations are essentially identical to the CBCCSP values.

Calibration of VIC was completed as part of the CBCCSP but was primarily focused on large drainages in the Columbia River Basin (Hamlet, et al., 2012). Specific calibration was not performed for the Skagit and Nisqually watersheds; therefore the routed VIC flows required bias correction in order to be used as inputs to the reservoir models (Hamlet, et al., 2010). A simple quantile mapping approach was used to adjust the daily flows produced by VIC. The quantile mapping approach forces the modeled daily flows to match the observed monthly and annual quantiles while preserving the daily time series signal produced by the VIC model. This bias correction process is similar in some ways to the hybrid-delta downscaling approach discussed above, but maps from CDFs of simulated values to CDFs of observed values.

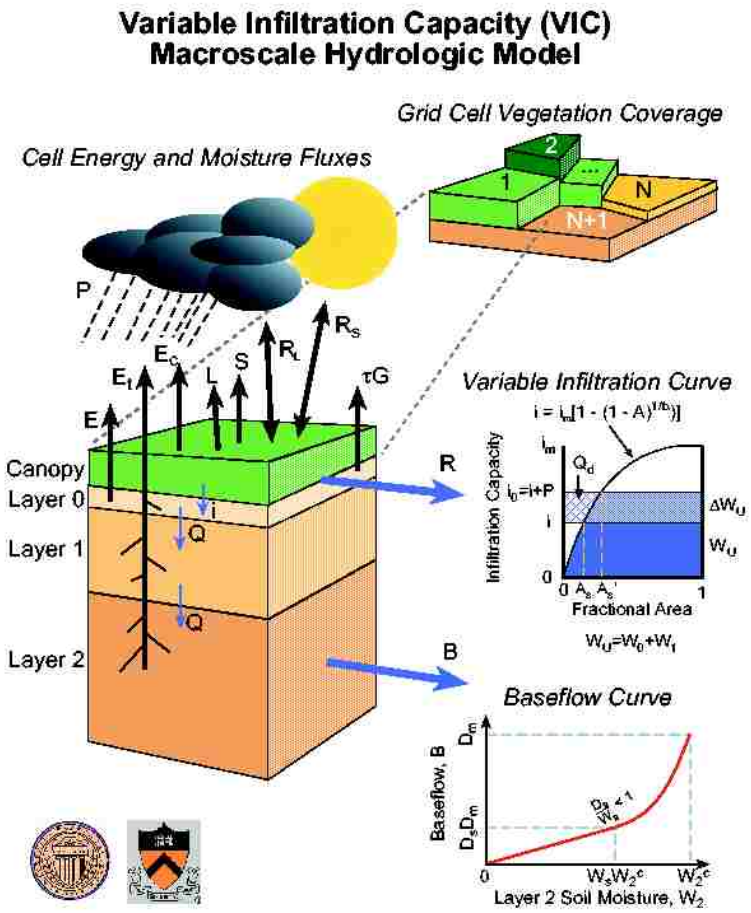

Figure 6 - Schematic diagram showing the basic structure of the VIC model. Source: Gao, et al., (2010)

3.5 Reservoir Modeling

The reservoir models used for the Skagit and Nisqually Rivers were implemented in the STELLA simulation modeling package (ISEE, 2012) using reservoir simulation algorithms developed by Hamlet (1996) and further described by Hamlet & Lettenmaier, (1999). The Skagit reservoir model used here was developed by Lee & Hamlet (2011). The methods and calibration techniques used for the Skagit model were also used to develop the Nisqually model constructed specifically for this project. The basic concepts driving the reservoir operations models are as follows:

1. Satisfy system mass balance (In – Out + $\Delta_{Storage}$ = 0), and physical constraints on reservoir storage and reservoir releases.
2. Satisfy local minimum flow requirements at each time step (when possible).
3. Satisfy hydropower production demands at each time step according to monthly and annual hydropower targets (which are a function of observed seasonal electrical power demand). Future demand is subject to seasonal and inter-annual variability that is accounted for relative to the mean April – September flow.
4. Follow flood control rules (e.g. flood rule curves and other operational procedures) and mimic flood control operations at daily time scales during simulated high flow events.

The reservoirs on the Skagit River operate specifically for flood control during large flow events. The reservoirs on the Nisqually River operate primarily for hydropower production but do provide some incidental flood control benefits. To model this difference a strict draw down curve was applied to the Skagit River reservoirs while a more flexible draw down schedule is followed in the Nisqually River reservoirs in order to prepare for the flood season. For the Nisqually reservoirs, during normal periods the model follows the soft rule curve. During flood events the model will not spill unless the reservoir is completely full, even if the level in the reservoir is above the soft rule curve. This modification added some skill to modeling reservoir operation in the Nisqually; although some difficulty still remains in completely capturing the observed flood operations (e.g. the model has the tendency to produce extremely large floods because it fills too quickly in some simulated future storms).

Figure 7 shows the probability distributions of peak annual flow at for each reservoir system including the two historical model runs and the observed USGS record. Overall, the models do a good job of representing reservoir behavior. Some of the bias in the CDFs shown below is due to bias inherited from the hydrology model. The remainder is reflective of the models' inability to perfectly capture flood dynamics. In the Skagit for example, the model was calibrated using the USGS gauge at Concrete. Incremental flows were applied to the reach between Concrete and Mt. Vernon. This step introduces some bias due to the lack of routing capabilities of the reservoir model. Furthermore, in longer historical runs (e.g. 1916-2003), both models do a much better job of replicating the observed CDF indicating that some of the bias in these shorter runs may be coming from errors associated with sample size. Steps to account for this model bias are described in section 3.7.

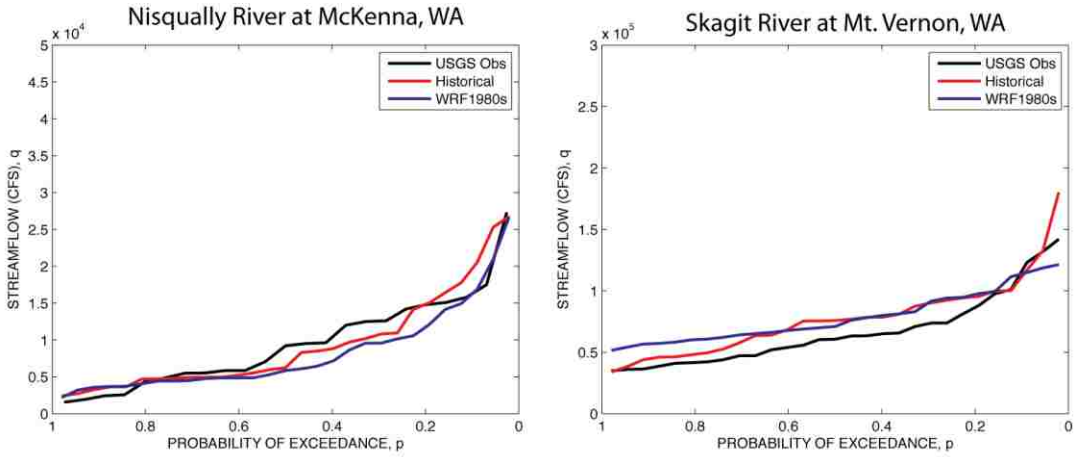

Figure 7 – Probability of exceedance of regulated peak annual flow for A) the Nisqually River at McKenna and B) the Skagit River at Mt. Vernon.

3.6 Sea Level Rise and Storm Surge Modeling

Estuarine flooding can be caused by a combination of unusually high base sea levels (e.g. during warm ENSO years or as a results of climate change related sea level

rise), storm surge, tide levels, and/or extreme river flow. A sea level and storm surge model was developed using a linear regression approach to quantify the effects of sea level rise and storm surge on coastal flooding and backwater conditions that partly determine river stage in the tidally influenced zone. The following steps were taken to predict future water levels.

1. Deriving Tidal Anomalies – Using NOAA hourly water levels, a least squares approach was used to fit the principle harmonic tidal constants using the T_Tide Matlab package (R. Pawlowicz, 2002). These constants were then used to predict hourly tides for the same time period (figure 8). The differences between the predicted and measured tides were summarized at a daily time step and separated by month.

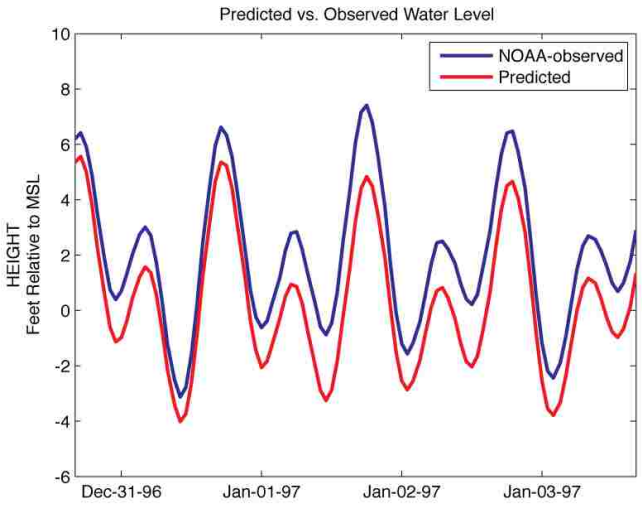

Figure 8 - Predicted vs. observed water levels during storm surge event from December 31, 1996 to January 3, 1997. Anomalies were calculated as the difference between the two curves.

2. Developing Model Inputs – All inputs to the regression model were derived directly from the GCM or dynamically downscaled RCM output with the exception of the historical Niño3.4 monthly time series which was derived from

the OISST.v3 gridded SST data. Local surface pressure was extracted from the RCM output at the grid cell centered over Seattle (48.3°N, -122.3°E). The raw surface pressure time series was aggregated from a 6-hour to 24-hour timestep.

A singular value decomposition (SVD) analysis was also performed on standardized daily surface pressure anomalies from the WRF reanalysis data (figure 9). The principal components of the first and third EOFs, explaining 30.78% and 12.26% of the variance in the pressure field respectively, were used as explanatory variables in the storm surge regression model. For the climate change values, the gridded RCM/ECHAM-5 outputs were projected onto the spatial EOFs and singular values of the reanalysis decomposition yielding the principle component time series for future climate projections associated with the observed spatial patterns. Further explanation regarding the use of the singular value decomposition techniques can be found in Appendix A.

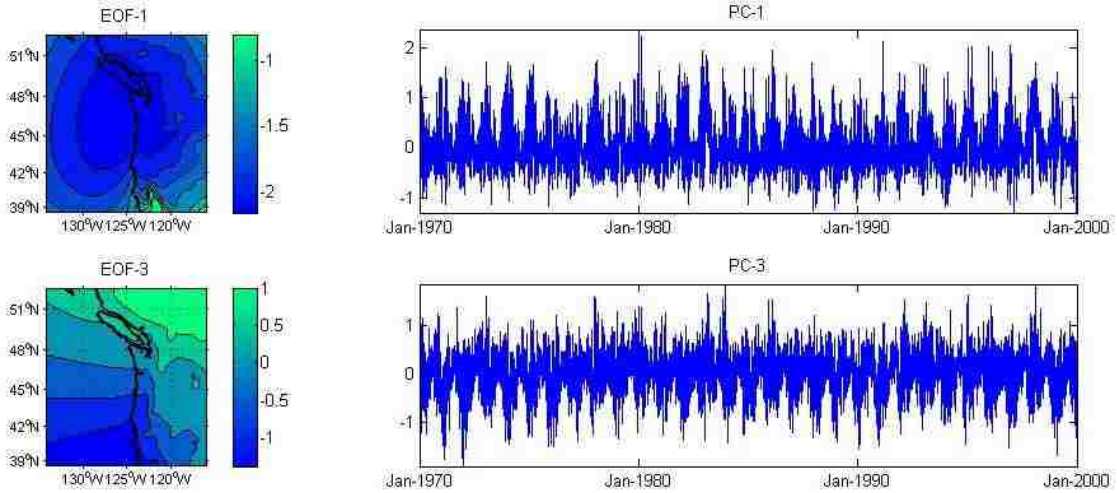

Figure 9 - First and third EOFs derived from gridded WRF-Reanalysis output from 1970-1999.

The historic monthly timeseries of the ENSO (Niño 3.4) index was also used to train the model (figure 10A). For the climate change scenario, the sea surface temperatures (SSTs) from the ECHAM-5/MPI-OM coupled land/ocean GCM were used to calculate the Niño 3.4 value for each future month using the methods described by Trenberth (1997) (figure 10B). Further discussion on the ENSO signal and the extraction of the Niño3.4 index from the GCM can be found in Appendix B.

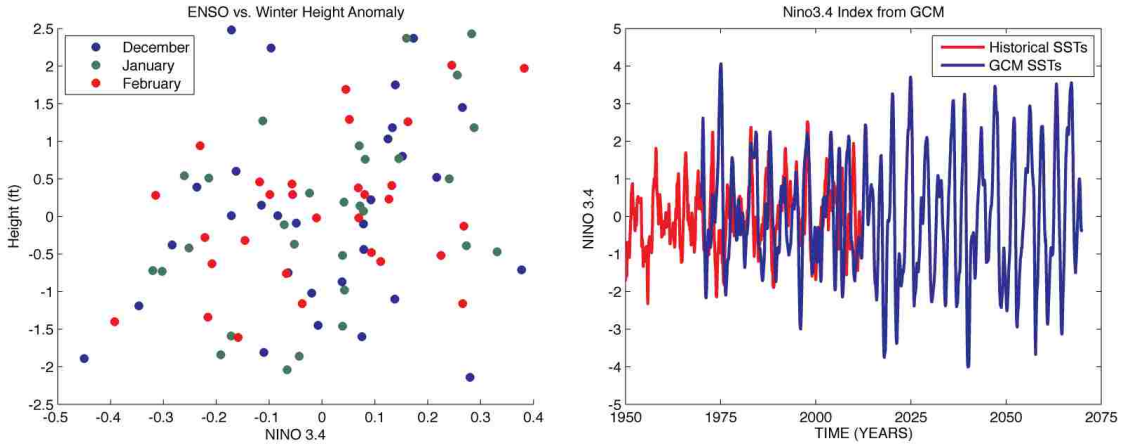

Figure 10 – A) Relationship between ENSO and mean monthly tidal anomaly for Seattle, WA (1970-1999). B) Observed Niño3.4 index (red), 1950-2012, and transient GCM derived Niño3.4 index (blue), 1970-2069. Note that, although there is no expectation that these two time series should match, the statistics desribing the interannual variability should be and are similar.

3. Training the Regression Model – An iterative approach was used to determine which variables best describe observed tidal anomalies. Local pressure (daily and 3-day average), the 1st and 3rd principle component time series associated with the large-scale pressure SVD analysis, and the ENSO index were the only variables found to be statistically significant explanatory variables for the regression model. A separate regression model was constructed for each month to account for the seasonal nature of anomalies. Hence, the regression model was trained such that:

$$Tide_{Anomaly} = f\ (Pressure, Pressure_{3DayAverage}, PC1, PC3, ENSO)$$

This approach yielded a good fit, particularly considering the many factors affecting storm surge. For the winter months, when flooding is of greatest concern and when anomalies are the largest, $R^2>0.75$ is obtained using this model formulation.

4. Predicting Future Tidal Anomalies - Using the regression parameters found for the observed training period and the input variables extracted from the GCM and RCM, storm surges were calculated for the ECHAM-5 1970-2069 period.
5. Predicting Future Tides - An hourly time series of predicted future tides was created using the harmonic constants determined in step 1. The predicted tides were then adjusted by adding the predicted storm surges.
6. Sea Level Rise - Sea level rise was uniformly added to the tidal anomaly for each time period based on highest projections outlined by Mote et al. (2008). Their study included regionally specific analysis of future relative sea level rise, taking into account vertical land movement and other factors. Mote et al (2008) also accounted for the large variety of possible sea level rise projections in published literature by providing a range of possible projections relative to their likelihood and impact for 2050 and 2100.

The science behind SLR projections is changing rapidly, and published projections of SLR have changed markedly even since the 2007 IPCC report (which also underlies the Mote et al. 2008 study discussed above). In particular, recent studies have pointed to higher estimates of global SLR and a greater range

of uncertainty than those published in the 2007 IPCC report due to accelerated contribution from melting ice in Greenland and Antarctica. For example, Vermeer and Rahmstorf (2009) projected that global SLR could exceed 180 cm by 2100 (yellow bar in figure 11). In this study, in an effort to acknowledge both the regional projections that account for local factors, and the more recent higher global SLR projections, the "high-impact, low probability" projections of Mote et al. (2008) were used in this study and are shown as green boxes in figure 11. SLR values for each time period were determined by evaluating a quadratic fit to the values published by Mote et al. (2008).

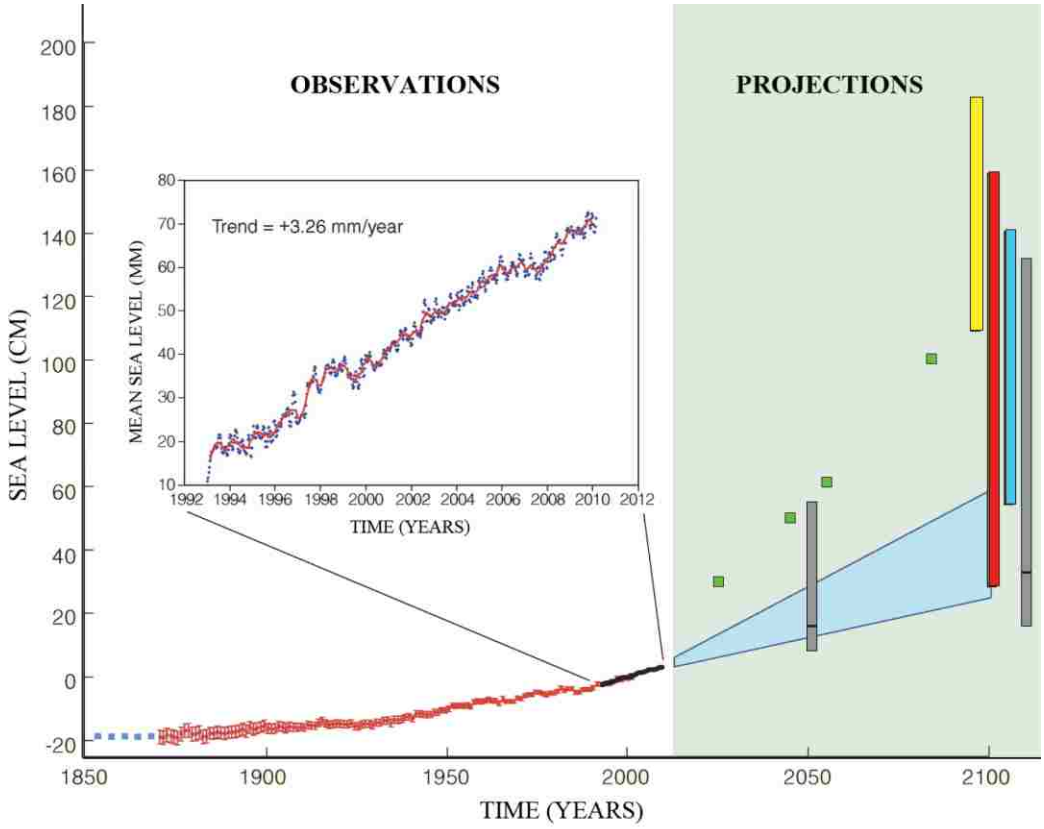

Figure 11 - Global mean sea level evolution of the 20th and 21st centuries. The red curve is based on tide gauge measurements. The black curve is the altimetry record. Projections for the 21st century are also shown. The shaded light blue zone represents IPCC AR4 projects for the A1FI greenhouse gas emissions scenario. Colored bars are semi-empirical projections for 2100. Grey bars are Puget Sound projections by Mote et al. (2008) for 2050 and 2100. Figure and caption adopted from Nicholls and Cazenave (2010) and Mote et al. (2008).

3.7 Hourly Disaggregation of Daily Flood Hydrographs

The hydrodynamic model used in the study (discussed below) required flow inputs at hourly time step in order to achieve computational stability. Temporal disaggregation to hourly time step was completed for flood events in the Skagit River. The *Steepness Index Unit Volume Flood Hydrograph Approach for Sub-Daily Flow Disaggregation* as described by Tan et al. (2007) assigns daily flood flows unit hourly hydrographs based on the steepness of the rising limb of the flood event. The assigned hydrograph is then scaled to match the four-day rising limb flood volume of the modeled daily flood. This method was chosen because it does not prescribe a certain hydrograph shape to all future flood events, rather it finds the closest approximation based on the characteristics of the simulated daily flood hydrograph, which could be substantially different in the future climate. In testing the approach on observed Skagit River floods, a reasonably accurate fit between observed and disaggregated hydrographs was achieved (figure 12A). Daily flows at Mt. Vernon simulated by the reservoir model were disaggregated to hourly hydrographs for all peak flow events that exceeded a 45,000 cfs threshold.

For a more direct comparison between the published FEMA 100-year storm and the future 100-year storm in the Skagit River, the historical hydrograph was simply scaled to match future peak flows. The scaling factor was defined the relative increase in 100-year flood volume indicated by the modeled hydrology for each time period. To determine the 100-yr peak flow, a Generalized Extreme Value Distribution was fit to modeled peak flows for each time period. For example:

$$FEMA2050s = FEMA \times \frac{100yrWRF2050s}{100yrWRF1980s}$$

This provided the direct comparison of flood dynamics in the Skagit Basin relative to the storm FEMA used in its floodplain mapping study of the same area (figure 12b). Table 6 shows the adjustment factors for each future time period. Results from both hourly disaggregation approaches are located in section 4.5.

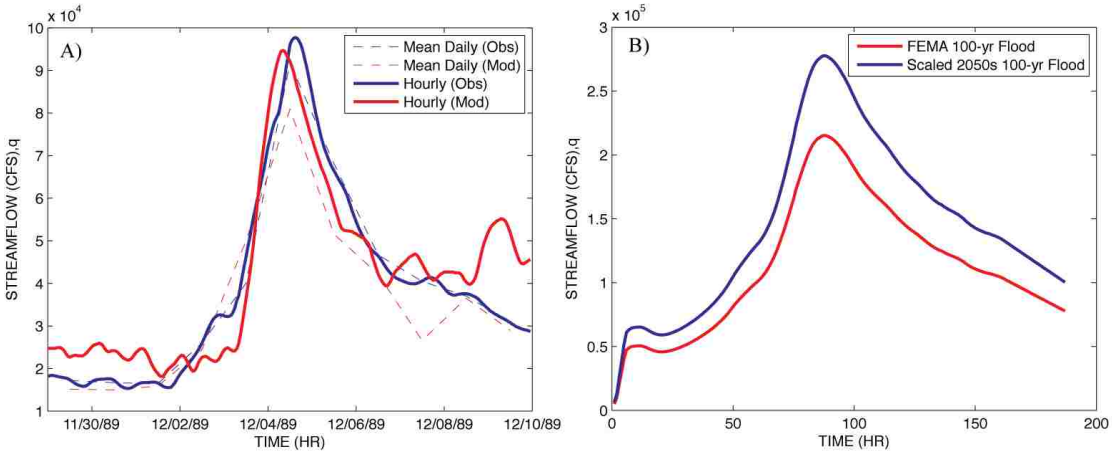

Figure 12- A) Example of disaggregated hourly flood event from December 5, 1989. Solid lines represent hourly hydrographs, dashed lines represent mean daily flow. B) Example of the 100-yr FEMA hydrograph (red) scaled by a factor of 1.29 for the 2050s (blue).

3.8 Hydrodynamic Modeling[2]

For the Skagit River portion of the project, a 2-dimensional (2D) hydrodynamic model (Flo2D) was implemented downstream of river mile 22.3. The Skagit model was developed as a combined effort between USACE and FEMA (USACE, 2007; USACE,

[2] Note: For the Nisqually River, a 2D/3D model (Delft 2D/3D) was implemented by USGS. Hydrodynamic modeling for the Nisqually is currently in progress and the results are not presented in this paper.

2008; USACE, 2009; FEMA, TBD). The model was constructed with a grid cell size of 400 ft. × 400 ft. Input data was delivered at an hourly timestep although the computation timestep was allowed to vary between 0.1 and 10 seconds. Due to levee conditions in the Skagit Basin, the floodplain model included seven levee failure scenarios used for flood risk mapping. Composite inundation maps were created by finding the maximum depth at each grid cell over the seven levee failure scenarios for specific zones outlined in the FEMA hydraulic report (figure C1). A summary of the floodplain mapping techniques used here and by the USACE and FEMA is located in Appendix C. The majority of the hydrodynamic model runs were completed only for the "No Levee Failure" scenario, although the scaled FEMA 2050s flood was evaluated for all seven levee scenarios. The benefits of using the same model combination as used by USACE/FEMA are that the results here can easily be compared to recent studies in the Skagit and the methods used to develop model inputs will be compatible with future studies.

3.9 Model Runs

The historical model run was set as the 30-year period centered around 1985. Gridded observations drove the hydrology model (Hamlet & Lettenmaier, 2005), and WRF-Reanalysis drove the storm surge model. This run was used to calibrate the storm surge and reservoir models and is used as a baseline for modeled changes in the hybrid delta runs. Sea level rise was assumed to be zero for this time period.

The dynamically downscaled climate model runs were split into three 30-year time blocks. These time periods are defined as the 1980s (centered around 1985), the 2020s (centered around 2025), and the 2050s (centered around 2055). For each of these

three time periods, all forcing came from the downscaled ECHAM5/WRF/VIC simulations. Sea level rise was uniformly added to each time period according to the predicted value at the middle of each period (1925 and 1955).

For the statistically downscaled runs, the hybrid delta method adjusted the time series behavior from the 1970-1999 period to match the 2040s and 2080s climate (mean changes of the 30yr period centered at 2045 and 2085 respectively). The results of the hybrid delta runs are provided to give better context to the changes in streamflow projected by the Regional Climate Model. Furthermore, based on the results described in section 4.3 in which negligible changes in the storm surge probability distribution are found, streamflows resulting from statistically downscaled GCM forcings are paired with storm surges derived from reanalysis. Because the time series associated with the statistically downscaled time periods originates in the 1980s, temporal consistency is maintained between the hydrologic forcings and the storm surge forcings by using WRF-reanalysis from the 1980s time period. Sea level rise was uniformly added to each time period according to the predicted value at the middle of each period (1945 and 1985).

Table 3 – Description of model runs. A total of six 30-year periods were analyzed using a combination of hybrid-delta and dynamic downscaling techniques. To provide temporal consistency between the hybrid-delta inputs and the storm surge forcings, the WRF-reanalysis was used for the HD-2040s and HD-2080s.

Time Period	Climate Scenario	Hydrologic Source	Storm Surge Source	Sea Level Rise (cm)	Description
1970-1999	Historic	Gridded Observations	WRF - Reanalysis	0	
1970-1999	HD-2040s	H.D. - ECHAM5 - 2040s	WRF - Reanalysis	49.17	Hybrid Delta 2040s using WRF reanalysis as time consistent storm surge forcings.
1970-1999	HD-2080s	H.D. - ECHAM5 - 2080s	WRF - Reanalysis	103.3	Hybrid Delta 2080s using WRF reanalysis as time consistent storm surge forcings.
1970-1999	ECHAM5-1980s	WRF	WRF – ECHAM5	0	WRF - ECHAM5 20th century climate run.
2010-2039	ECHAM5-2020s	WRF	WRF – ECHAM5	28.51	WRF - ECHAM5 SRES A1B, 2010 – 2039.
2040-2069	ECHAM5-2050s	WRF	WRF – ECHAM5	61.1	WRF - ECHAM5 SRES A1B, 2041 – 2069.

4 Results

4.1 Unregulated Hydrology

A number or previous climate change impacts studies have shown that warming in the PNW will lead to larger flood events on the west slopes of the Cascades (Hamlet, et al., 2009; Lee, et al., 2009; Hamlet, et al., 2010; Lee, et al., 2011). This is especially true in transient mixed rain/snow basins where the flooding can be buffered by snow accumulation at higher elevations during storms (Hamlet & Lettenmaier, 2007). The majority of the increases in flood magnitude simulated by the hybrid delta approach are due to increases in temperature (increased basin area) and, to a smaller extent, increasing cool season precipitation (Hamlet & Lettenmaier, 2007). RCM simulations demonstrate that climate change may enhance extreme precipitation events on the windward slopes of the Cascades (Salathé et al., 2010; Duliere, et al., 2011). These effects are included in the ECHAM5/WRF/VIC simulations.

A useful way to look at systemic changes in flood behavior is through probability distributions. In figure 13, peak annual unregulated flow for the Sauk River[3] and Nisqually River at Alder Dam are plotted using the Cunnane unbiased quantile estimator (Cunnane, 1978). The largest increases are found in those events occurring once or twice per decade. The hybrid-delta runs show slightly larger increases in flood magnitude than the RCM relative to the historical run associated with that model run (i.e. the WRF runs are compared to the WRF 1980s, not the historical run).

[3] The Sauk River is a major unregulated tributary to the Skagit River. The principle basin characteristics (e.g. topography, elevation, land cover, location, etc.) are essentially the same between the main stem of the Skagit and the Sauk. It is used here as an analog for the unregulated Skagit River due to the absence of bias corrected unregulated flows elsewhere in the basin.

Table 4 – 5, 10 and 100-year unregulated events for the Nisqually River at Alder Dam and the Sauk River near Sauk, WA for each model run calculated using a generalized extreme value distributions fit for each 30-year time period. The percentages in columns 3, 5, and 7 are the increases relative to historical period of that model (i.e. WRF-2050s is relative to the WRF-1980s).

	Nisqually River					
	p=0.2		**p=0.1**		**p=0.01**	
Historic	13,989		17,232		29,119	
HD-2040s	16,009	(1.14)	19,162	(1.11)	29,383	(1.01)
HD-2080s	17,560	(1.26)	21,801	(1.27)	37,699	(1.29)
WRF-1980s	14,240		18,183		35,920	
WRF-2020s	16,959	(1.19)	23,064	(1.27)	57,166	(1.59)
WRF-2050s	16,985	(1.19)	20,334	(1.12)	30,532	(0.85)
	Sauk River					
	p=0.2		**p=0.1**		**p=0.01**	
Historic	30898.9		38627.2		72820	
HD-2040s	40670.6	(1.32)	49479.4	(1.28)	81442.6	(1.12)
HD-2080s	50681.7	(1.64)	59267.8	(1.53)	84629.4	(1.16)
WRF-1980s	29,914		36,380		64,953	
WRF-2020s	34,829	(1.16)	44,045	(1.21)	94,552	(1.46)
WRF-2050s	41,418	(1.38)	49,971	(1.37)	78,837	(1.21)

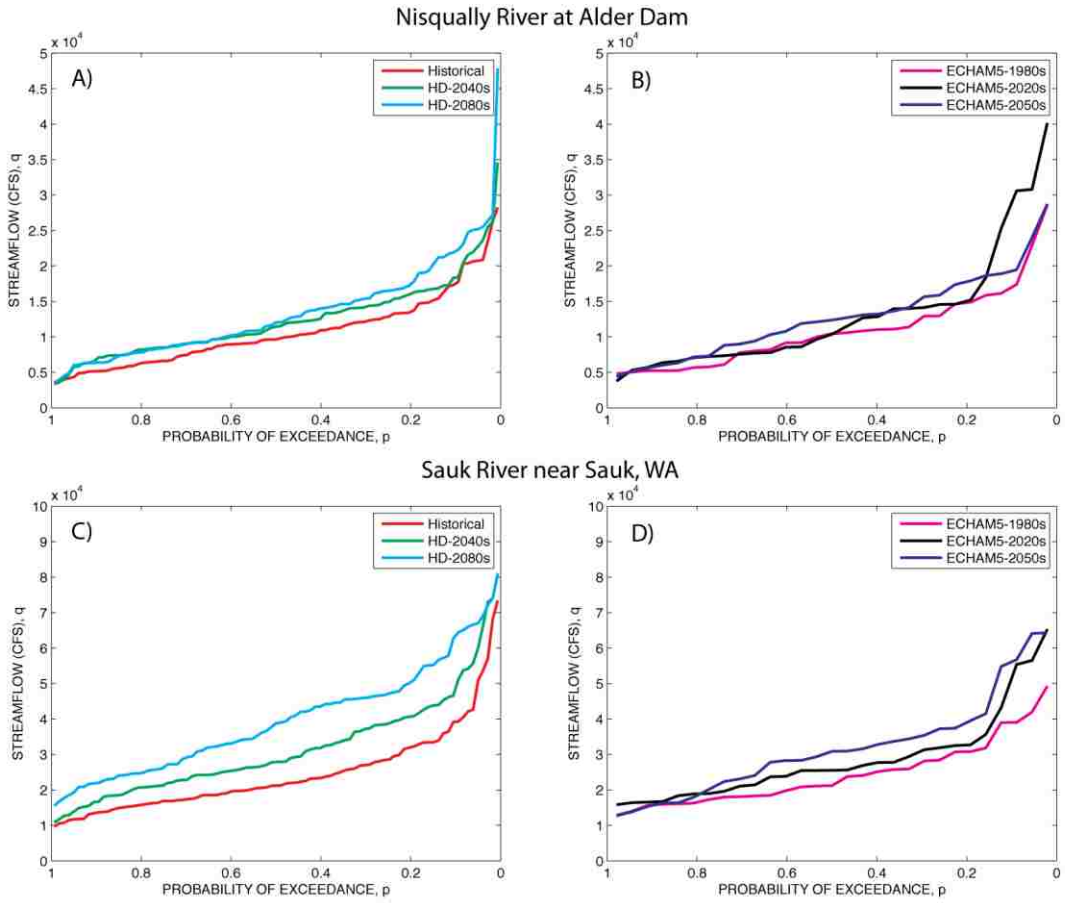

Figure 13 - Probability of exceedance of unregulated peak annual flow for the Nisqually and Sauk Rivers plotted using the unbiased Cunnane quantile estimator.

Figure 14 shows the date of peak annual flow for the two locations shown in figure 13. Historically, the largest flooding events have occurred in the late fall and early winter with a few smaller events occurring during the spring melt. Based on the results from both the statistically and dynamically downscaled runs, there is some evidence to support fewer spring events in the future due to a shift towards larger winter floods, resulting from higher freezing lines and increasing precipitation, smaller winter snowpack and earlier melt dates in spring.

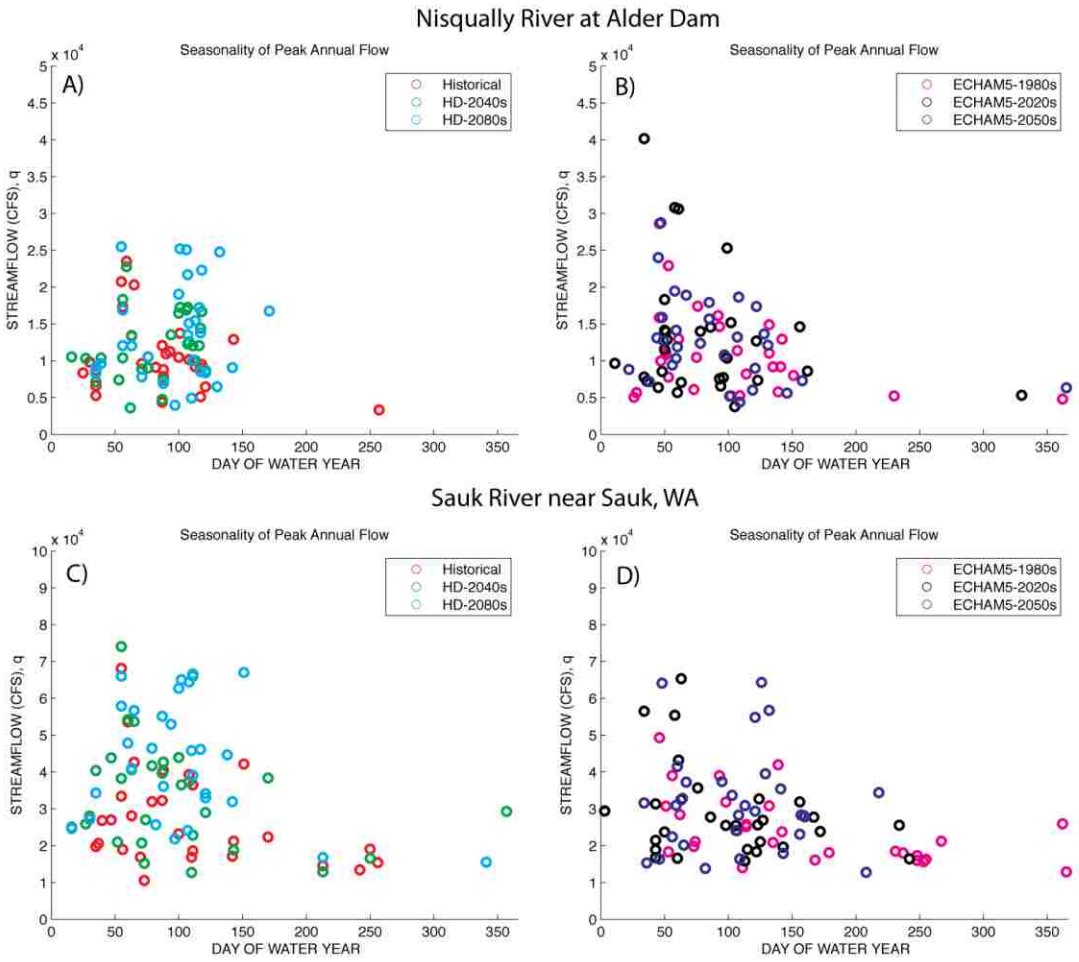

Figure 14 - Scatter plot of peak annual streamflow (y-axis) and date of occurrence (x-axis).

4.2 Regulated Hydrology

Figure 15 shows the CDFs of peak annual regulated flow for the Skagit and Nisqually Rivers. Qualitatively the results look similar to those presented in the previous section. In cases where there is some potential elasticity in reservoir operations, modeled increases may be partially offset by new reservoir operations (Lee, et al., 2009). Lee and Hamlet (2011) showed that because there are major unregulated tributaries which contribute to flooding in the lower basin, (particularly the Sauk), modifying flood rule curves provides little buffering against predicted increases in flood risk. The same may

not be true in the Nisqually River Basin because there are no major unregulated tributaries and the reservoirs are not currently operated for flood control.

Table 5 – 5, 10 and 100-year unregulated events for the Nisqually River at McKenna and the Skagit River at Mt. Vernon for each model run calculated using a generalized extreme value distributions fit for each 30-year time period. The percentages in columns 3, 5, and 7 are the increases relative to historical period of that model (i.e. WRF 2050s is relative to the WRF-1980s). Grey highlighting indicates poor fit for the GEVD compared to Cunnane unbiased quantile estimates.

	Nisqually River at McKenna, WA					
	p=0.2		**p=0.1**		**p=0.01**	
Observations	13,662		17,614		31,734	
Historic (% Obs)	12,597	(0.92)	18,530	(1.05)	59,774	(1.88)
HD-2040s (% His)	15,103	(1.20)	22,529	(1.22)	74,932	(1.25)
HD-2080s (% His)	18,579	(1.47)	46,327	(2.50)	1,138,838	(19.05)
WRF-1980s (% Obs)	10,722	(0.78)	15,202	(0.86)	43,965	(1.39)
WRF-2020s (% 1980s)	13,082	(1.22)	24,434	(1.61)	228,746	(5.20)
WRF-2050s (% 1980s)	15,927	(1.49)	23,657	(1.56)	77,055	(1.75)
	Skagit River at Mt. Vernon, WA					
	p=0.2		**p=0.1**		**p=0.01**	
Observations	82837.4		105948.6		231087.36	
Historic (% Obs)	98317.4	(1.19)	116762.4	(1.10)	178796.44	(0.77)
HD-2040s (% His)	126439	(1.29)	148309.3	(1.27)	220554.38	(1.23)
HD-2080s (% His)	134070	(1.36)	157285	(1.35)	237538.02	(1.33)
WRF-1980s (% Obs)	91850.8	(1.11)	106805.4	(1.01)	170333.49	(0.74)
WRF-2020s (% 1980s)	102378	(1.11)	119537.8	(1.12)	189438.13	(1.11)
WRF-2050s (% 1980s)	118506	(1.29)	139298.1	(1.30)	219787.76	(1.29)

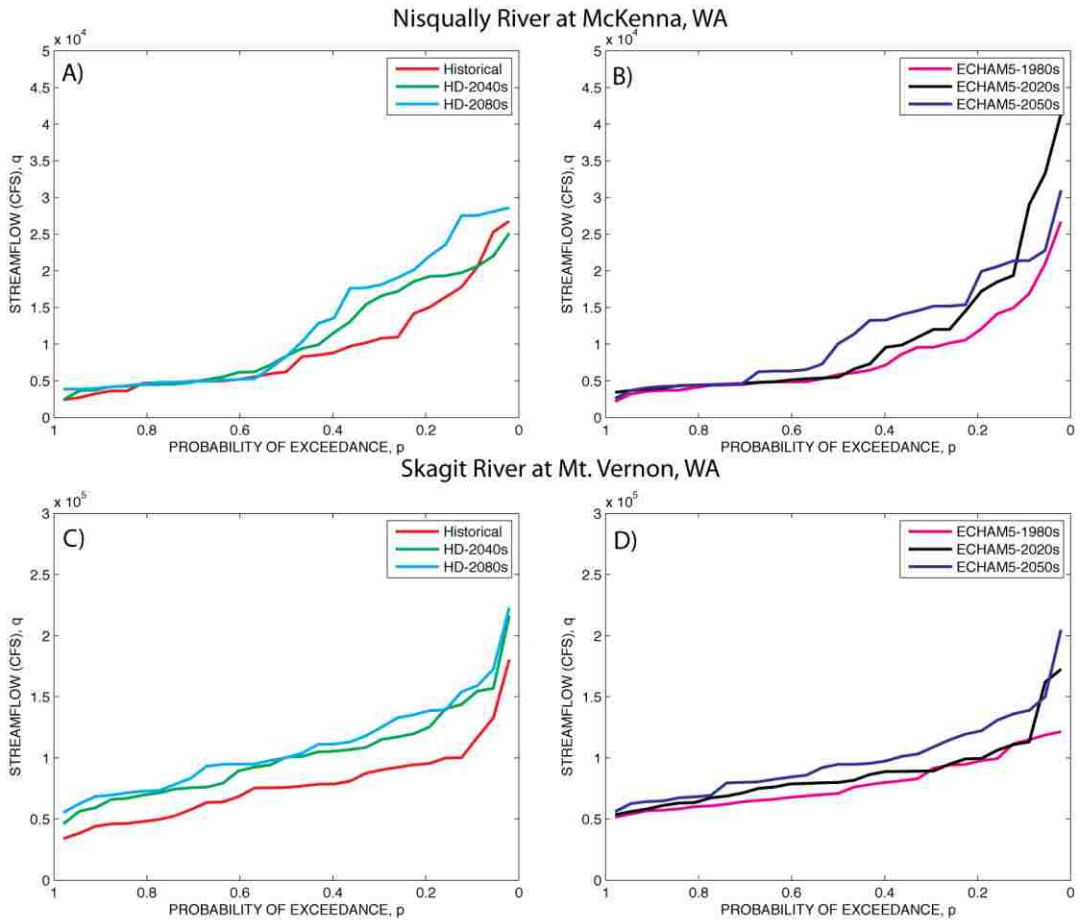

Figure 15 – Probability of exceedance of regulated peak annual streamflow for the Nisqually and Skagit Rivers. The relatively common storms 1>p>0.6 experience little change in the Nisqually demonstrating the capacity of reservoir operations to control smaller floods. The Skagit does not show the same flexibility. Both Rivers experience significant increases in the 0.4>p>0.1 peak flows.

4.3 Sea Level and Storm Surge

Climate change is expected to cause relatively little change, if any, in storm surge (Stammer & Huttemann, 2008). These results confirm this hypothesis. Figure 16a shows the maximum annual mean daily storm surge at Seattle for the four model runs: WRF-Reanalysis, RCM-1980s, RCM-2020s, and RCM-2050s. Three observations are immediately apparent from this figure, 1) there are only minor variations between the three ECHAM-5 model runs indicating no systemic shift in storm surge forcings due to climate change, 2) there is a small positive bias in the ECHAM-5 runs for the largest

events relative to the reanalysis run, indicating that the WRF model may produce slightly larger storms than have historically been seen, and 3) there is a fairly small range of storm surges between the 1-yr and 100-yr events (about 1.5-ft). The PNWs lack of large storm surge events (e.g. tropical storms) indicates that sea level rise, rather than storm surges, will more significantly alter the future probability distribution of this region (Tebaldi, et al., 2012).

The sea level rise impacts on peak storm surge are clearly seen in figure 16b. In this figure, the 1-yr storm surge event of the 2050s exceeds the 100-yr event of the 1980s. Along with this intense increase in peak surge levels, similar increases are found when the tidal signal is included. In the Puget Sound, the range within the tidal cycle is nearly an order of magnitude larger than that of the observed storm surge, and the size of the storm surge does not change significantly with climate change. Adding 2-3 feet of sea level rise to typical high tides is likely to bring significant damage to low-lying areas in the Puget Sound.

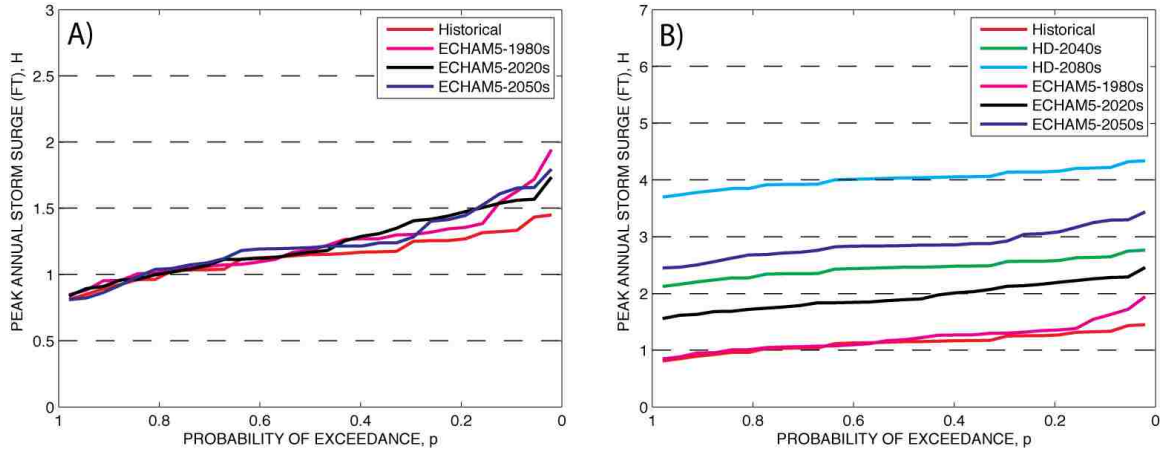

Figure 16 – A) Probability of exceedance of peak annual storm surge relative to 1980s mean sea level. Peak storm surges created by the RCM slightly exceed historic values. Future storm surge distributions relative to the 1980s ECHAM-5 run are not expected to change. B) Peak annual storm surge including sea level rise relative to 1980s mean sea level. By the 2050s, the expected 1-yr peak storm surge is found to exceed the historic 100-yr level.

4.4 Coincident Occurrence of Flooding and Storm Surge

Combining temporally consistent riverine flooding and storm surge provides the ability to assess the likelihood of coincident events as they vary in time. This is especially important when considering the estuary and tidally influenced portions of the river channel. In some Puget Sound rivers, backwater conditions created by storm surges and extreme tides can affect riverine flood stage as far as 20 km upstream. Examining joint probability of exceedance in these variables is a crucial step in flood risk assessment. For example, excluding storm surge from flood risk modeling can lead to unrealistically low estimations of water levels. Conversely, pairing the 100-yr storm surge with the 100-yr flood may drastically over estimate water levels for the paired 100-yr event. In order to use these results effectively, the sensitivity of flooding relative to each variable must be well understood.

Figure 17 shows the coincident relationship between regulated peak annual streamflow and the paired tidal anomaly. This figure demonstrates a wide range of pairings in both river systems. Although there is a wide range of pairings, numerous future large flood events occurred during periods of depressed sea levels, an association not experienced in the historical run. Attributing a cause to this observation is difficult but may be the result of increased influence of the ENSO phenomenon on flooding (e.g. large floods in La Nina years with associated depressed sea levels) or altered storm dynamics (e.g. high pressure system follows large low pressure systems).

A positive trend relating these two variables is found in each model run. However, statistical inference testing cannot reject the null hypothesis (defined as the

slope of the best fit line equal to zero) at a 95% confidence interval. The absence of statistically significant relationship between storm surge and riverine flooding combined with the stationary behavior of the storm surge probability distribution further indicates that sea level rise will be the dominant driver in future tidal anomalies.

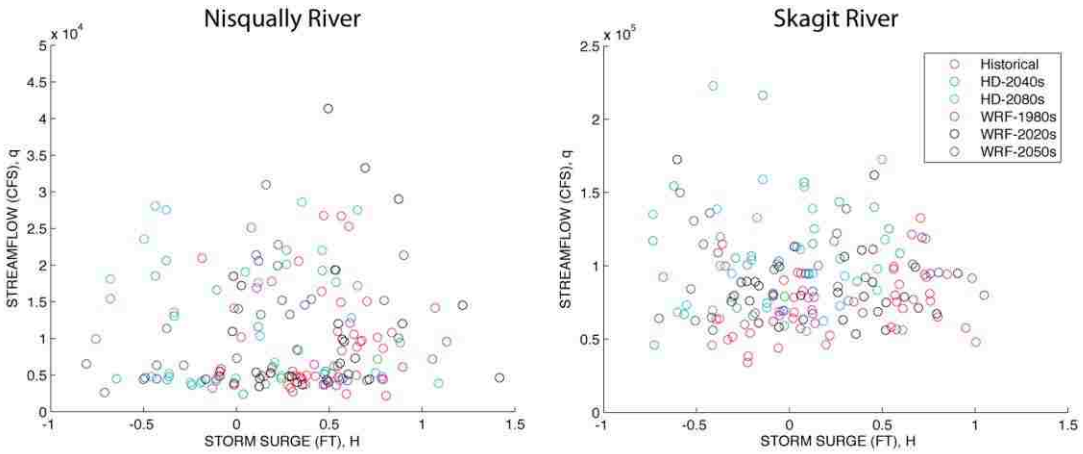

Figure 17 – Relationship between regulated peak annual streamflow (y-axis) and coincident tidal anomaly (x-axis) for A) the Nisqually River and B) the Skagit River. No statistically significant relationship was found in either river for any of the model runs.

4.5 Hydrodynamic Modeling Results for the Skagit River Basin

Two model runs were performed to assess the basin's sensitivity to single variable changes. Evaluating the FEMA hydrograph with projected 2050s SLR, inundated area increases from 42,266 acres to 57,043 acres. Larger increases are found when the 2050s scaled FEMA 100-yr flood is modeled without sea level rise where inundated area increased to 72,749 acres. In this case, inundated area is approximately equal to the combined SLR/increased flooding amount. This is likely because the size of the flood is so great that most of the floodplain is flooded based on flood volume alone. These changes in inundated area indicate that smaller future storms may create substantial inundated area due to rising sea level alone. Figure 19 compares the results of the sensitivity analysis.

Two approaches were used to model the physical dynamics of future flooding in order to consider the changes in flood volume, storm surge and sea level rise described above. To eliminate the bias in regulated flows shown in table 5, the FEMA 100-yr storm was scaled to reflect projected increases in the 100-year flood for each time period. Table 6 shows the amount of inundation for each of the scaled FEMA storms. Figure 19 shows the extent of inundation from the FEMA storm's "No Levee Failure" scenario. Figures 21-24 show the extent of inundation for the scaled FEMA storms' "No Levee Failure" scenario. These four runs (e.g. 2020s, 2040s, 2050s, and 2080s) resulted in increased inundation of 53%, 69%, 72%, and 75% relative to the historical FEMA storm. Figure 18 compares the changes in 100-yr flood volume and sea level rise to areal inundation in the Skagit River. Although, large increases are found by the 2020s and 2040s relative to the historical flood, lessening increases are experienced in the 2050s and 2080s runs. The diminishing inundations due to increased peak flow and sea level rise bring into question the capacity of the hydrodynamic model to resolve the impacts of these larger flood events.

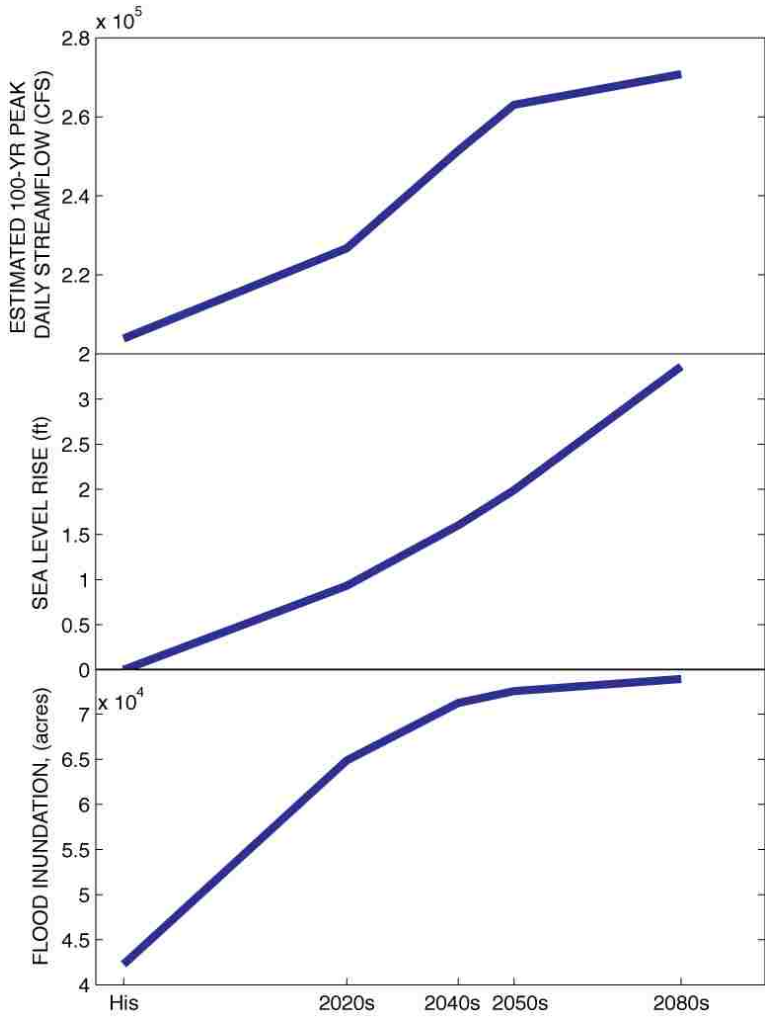

Figure 18 – Summary of hydrodynamic modeling results. The top two panels, extrapolated 100-yr peak daily flow sea level rise, represent inputs into the hydrodynamic model for each of the five modeled time periods (His, 2020s, 2040s, 2050s and 2080s). The bottom panel represents inundated area in the Skagit River basin for the "All Levees Intact" scenario.

Figure 25 shows a comparison between the composite flood map for all seven scenarios from the historical FEMA 100-yr flood and the 2050s scaled FEMA 100-yr flood. The results shown in the composite maps indicate that the 100-year flood depths in the lower Skagit River will be, on average, 10-inches higher in the 2050s than the historical case. The most significant increases in flood depth are seen in the area northeast of Mt. Vernon where increases in projected flood depths range from 3-5 feet.

In order to assess some of the dynamics of future flooding given paired changes in the riverine flooding and sea level/storm surge, an ensemble of the three largest storms experienced in the Skagit River during the RCM-2050s run were evaluated using the hydrodynamic model. These storms, paired with their corresponding tidal signal, were input into the hydrodynamic model for the "No Levee Failure" scenario. The largest flood of the 2050s run occurred on 1/30/2069 and had a peak daily flow of 204,718 cfs. Although this event is only slightly larger than the FEMA 100-yr event (<1%), the inundation created by the flood combined with SLR is approximately 43% greater. The second largest storm in the 2050s run occurred on 2/4/2053 and had a peak daily flow of 149,890 cfs. This storm created inundation approximately equal to the FEMA 100-yr event despite having a much smaller peak flow. Figures 27-29 show the input hydrograph, tidal signal, and inundation maps for each storm.

Naturally, larger peak flows and SLR equate to more extensive inundation. A summary of peak flow and inundated area is shown in table 6. It appears that even slight increases beyond the FEMA 100-yr event, such as the WRF-2020s event, create substantial increases in inundation. This indicates that the lower Skagit is fairly inelastic in its ability to handle the increases in peak flow due to climate change, thus these changes will have very large impacts on flood inundation.

Table 6 - Summary of hydrodynamic modeling results for the "No Levee Failure" Scenario.

Climate	Storm	Peak Daily Flow (cfs)	Peak Hourly Flow (cfs)	SLR (ft)	Inundation (acres)
Observed	FEMA	203,835	215,270	0.00	42,266
WRF-2020s	1.11*FEMA	226,697	239,415	0.93	64,878
HD-2040s	1.23*FEMA	251,441	265,546	1.60	71,236
WRF-2050s	1.29*FEMA	263,016	277,771	1.99	72,555
HD-2080s	1.33*FEMA	270,803	285,995	3.36	73,914
WRF-2050s	1/30/2069	204,718	221,416	1.99	60,544
WRF-2050s	2/4/2053	149,890	187,973	1.99	43,052
WRF-2050s	11/18/2047	138,945	162,376	1.99	22,527
Sensitivity	2050s SLR Only	203,835	215,270	1.99	57,043
Sensitivity	2050s Flood Only	263,016	277,771	0.00	72,749

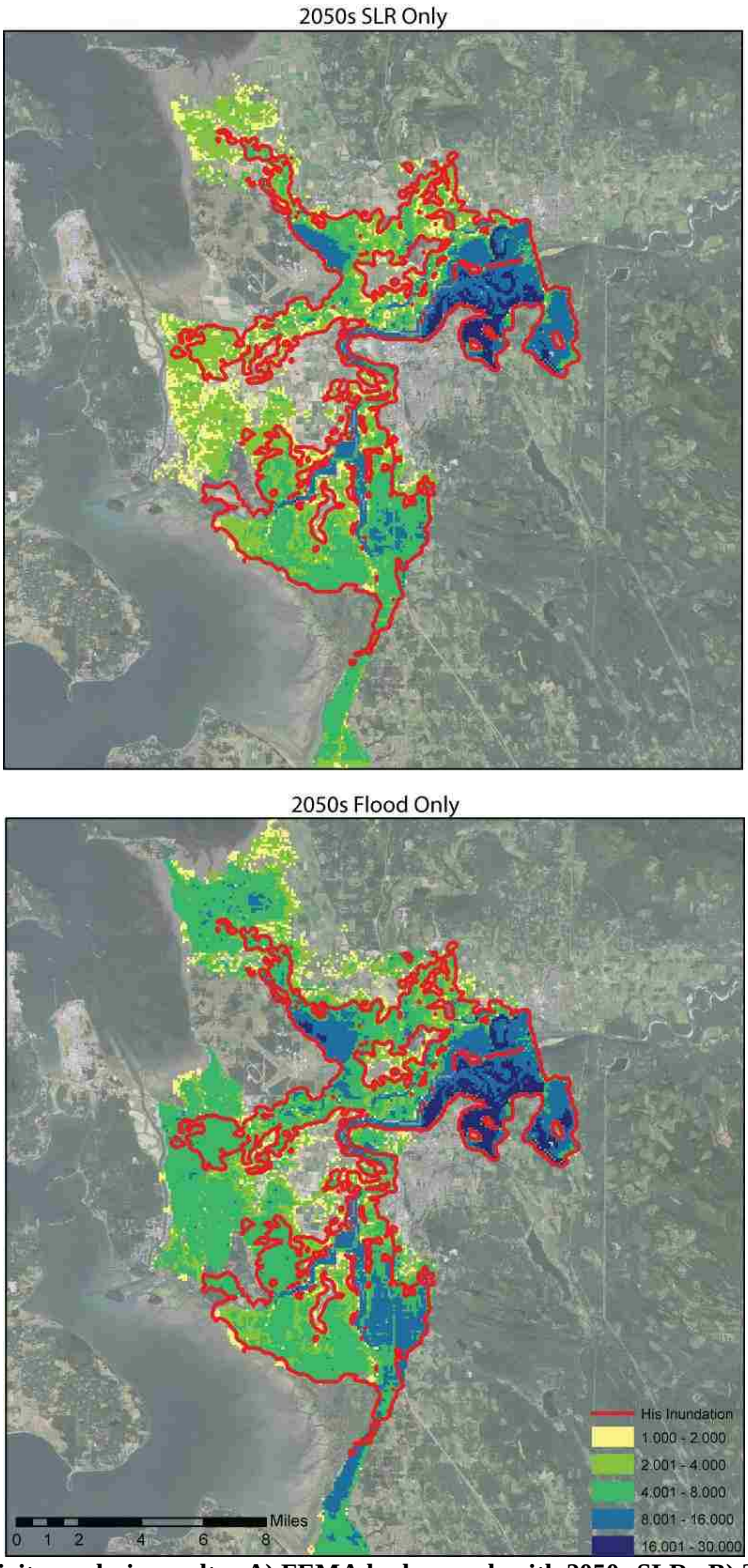

Figure 19 - Sensitivity analysis results. A) FEMA hydrograph with 2050s SLR. B) 2050s scaled FEMA hydrograph with historical tides. Red lines represent the historical FEMA 100-yr flood inundation. Units: Feet.

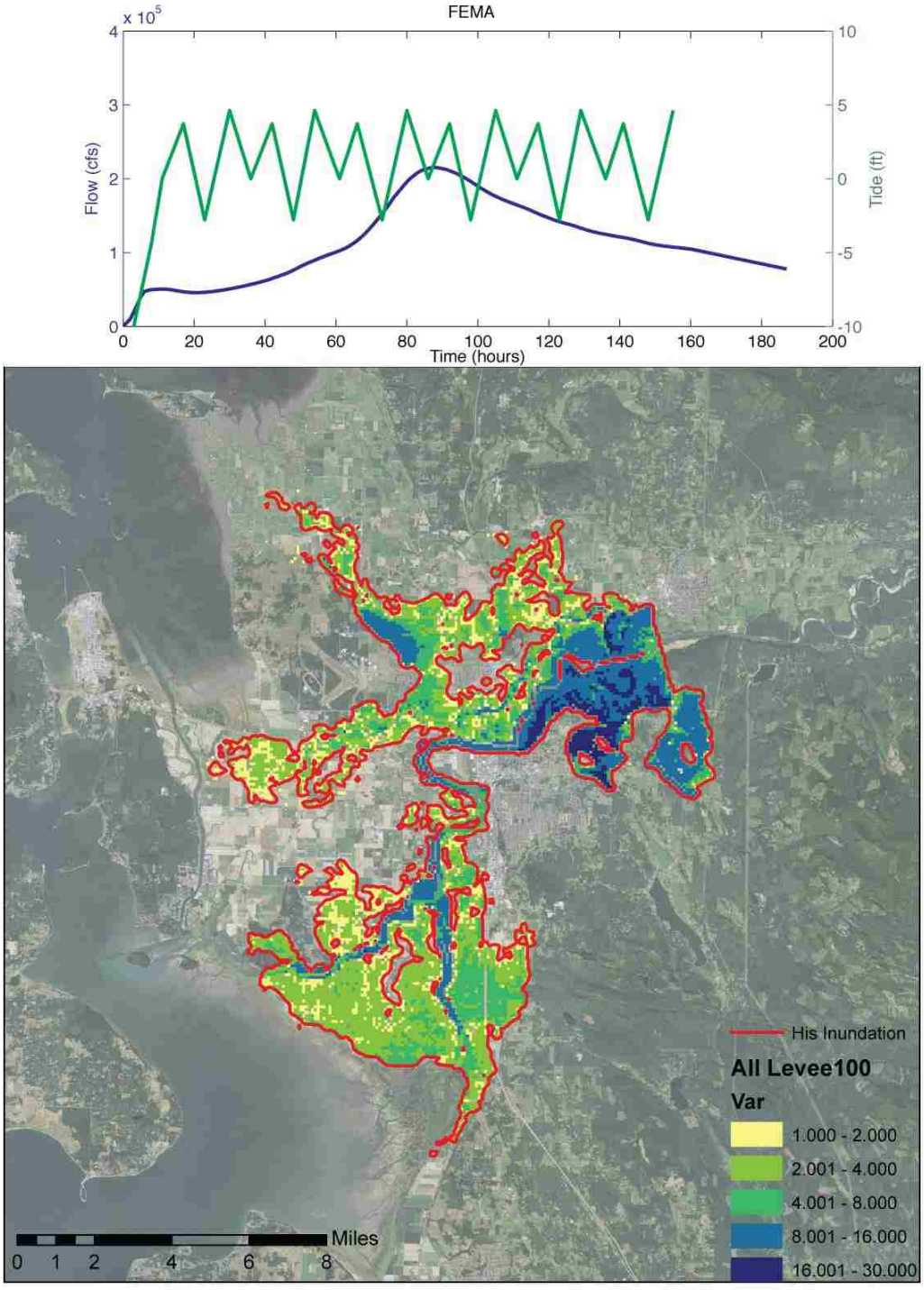

Figure 20 - Inundation map for FEMA storm for the No Levee Failure Scenario. The top panel represents the inflow and outflow boundary conditions. Red lines represent the historical FEMA 100-yr flood inundation. Units: Feet.

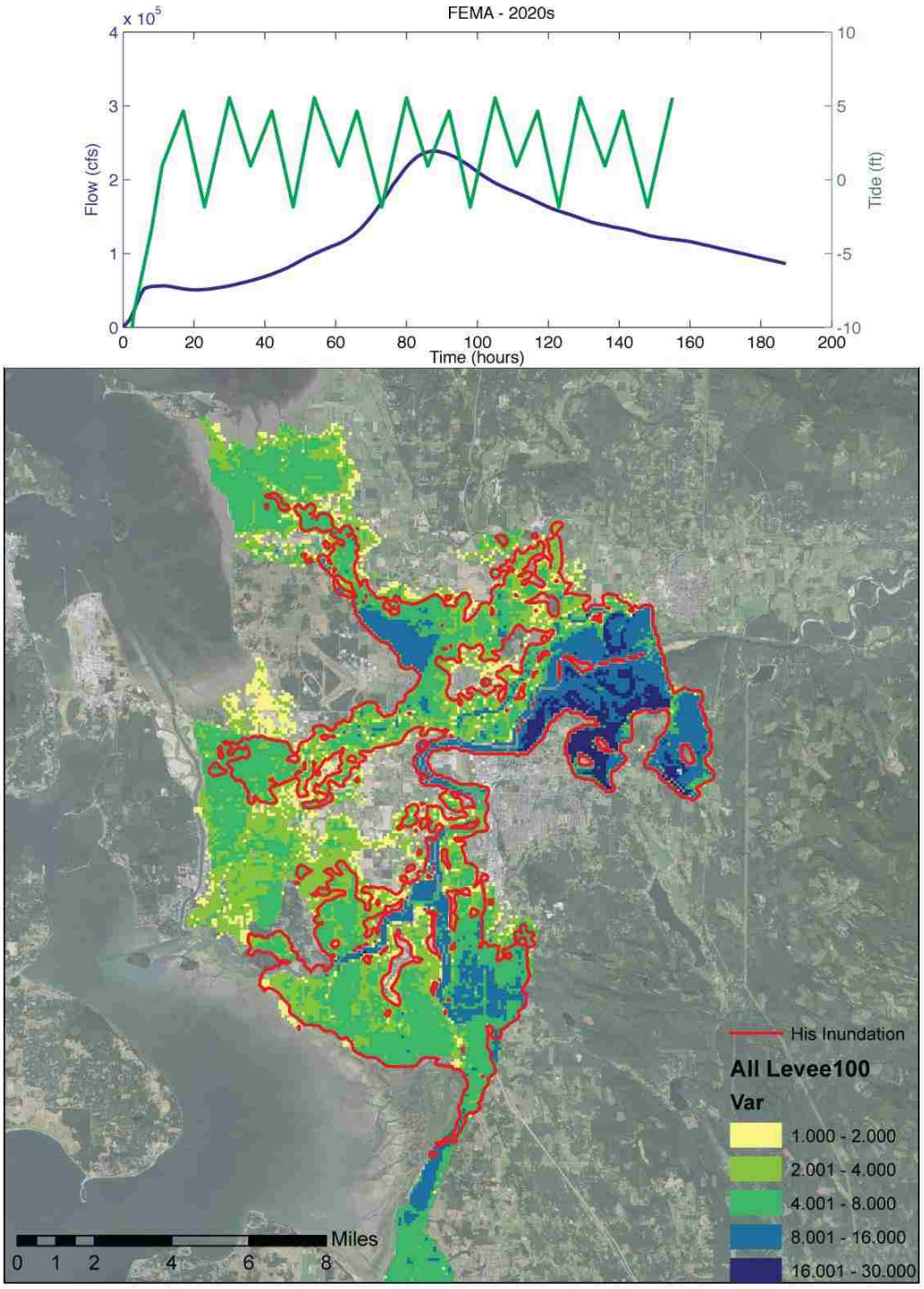

Figure 21 - 2020s scaled FEMA 100-yr inundation map for the "No Levee Failure" Scenario in the Skagit River Basin. Red lines represent the historical FEMA 100-yr flood inundation. The top panel represents the inflow and outflow boundary conditions. Units: Feet.

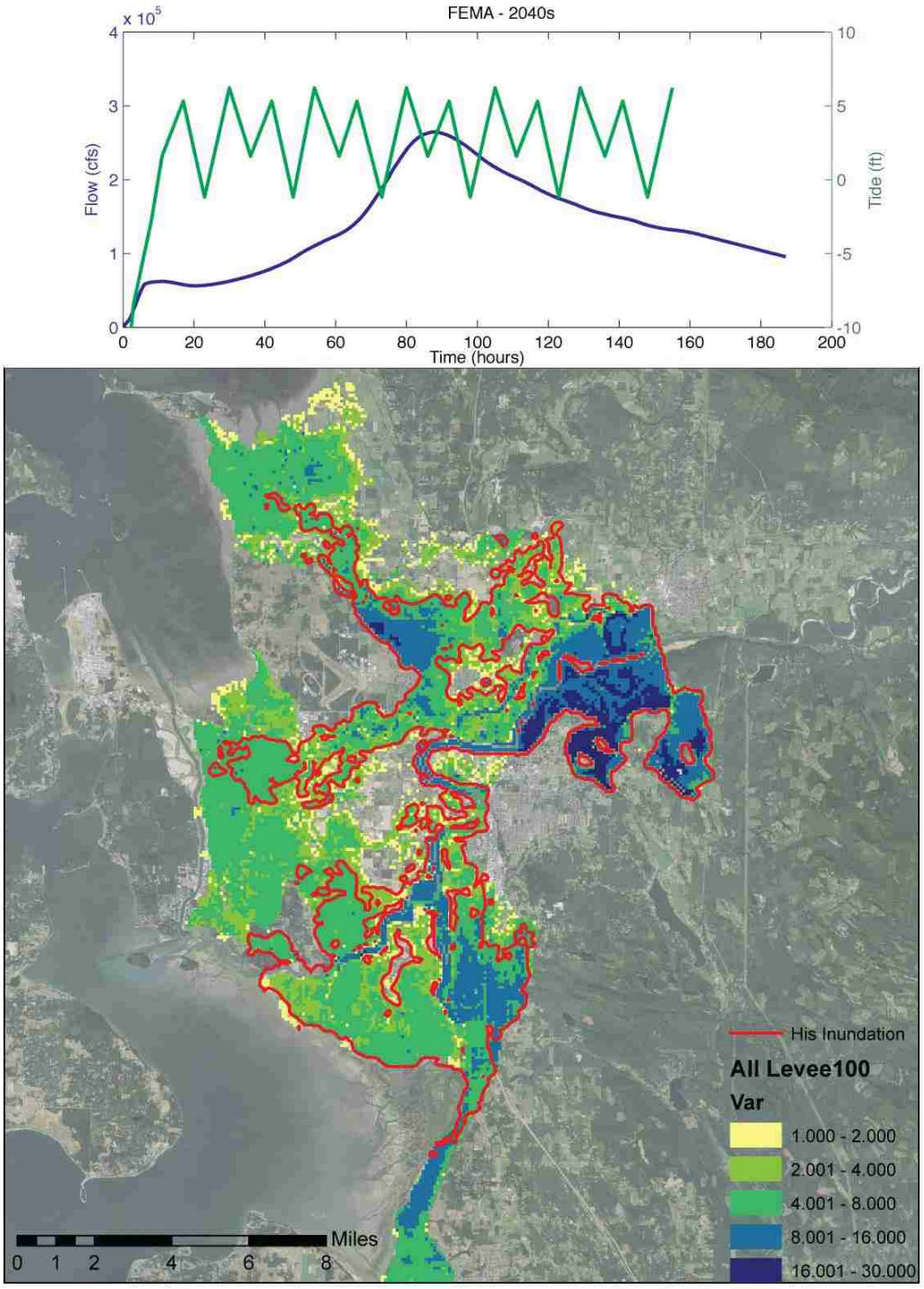

Figure 22 - 2040s scaled FEMA 100-yr inundation map for the "No Levee Failure" Scenario in the Skagit River Basin. Red lines represent the historical FEMA 100-yr flood inundation. The top panel represents the inflow and outflow boundary conditions. Units: Feet.

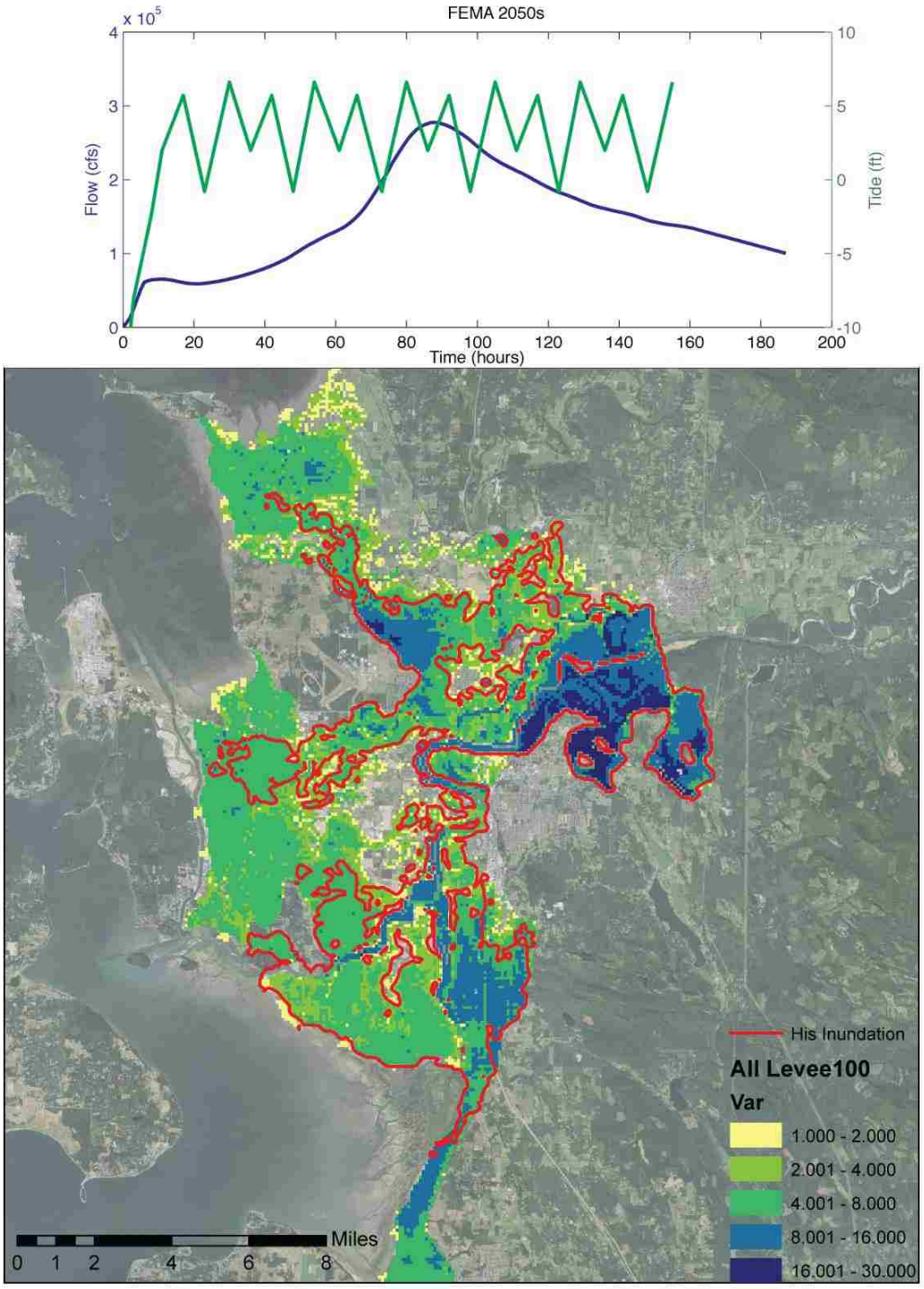

Figure 23- 2050s scaled FEMA 100-yr inundation map for the "No Levee Failure" Scenario in the Skagit River Basin. Red lines represent the historical FEMA 100-yr flood inundation. The top panel represents the inflow and outflow boundary conditions. Units: Feet.

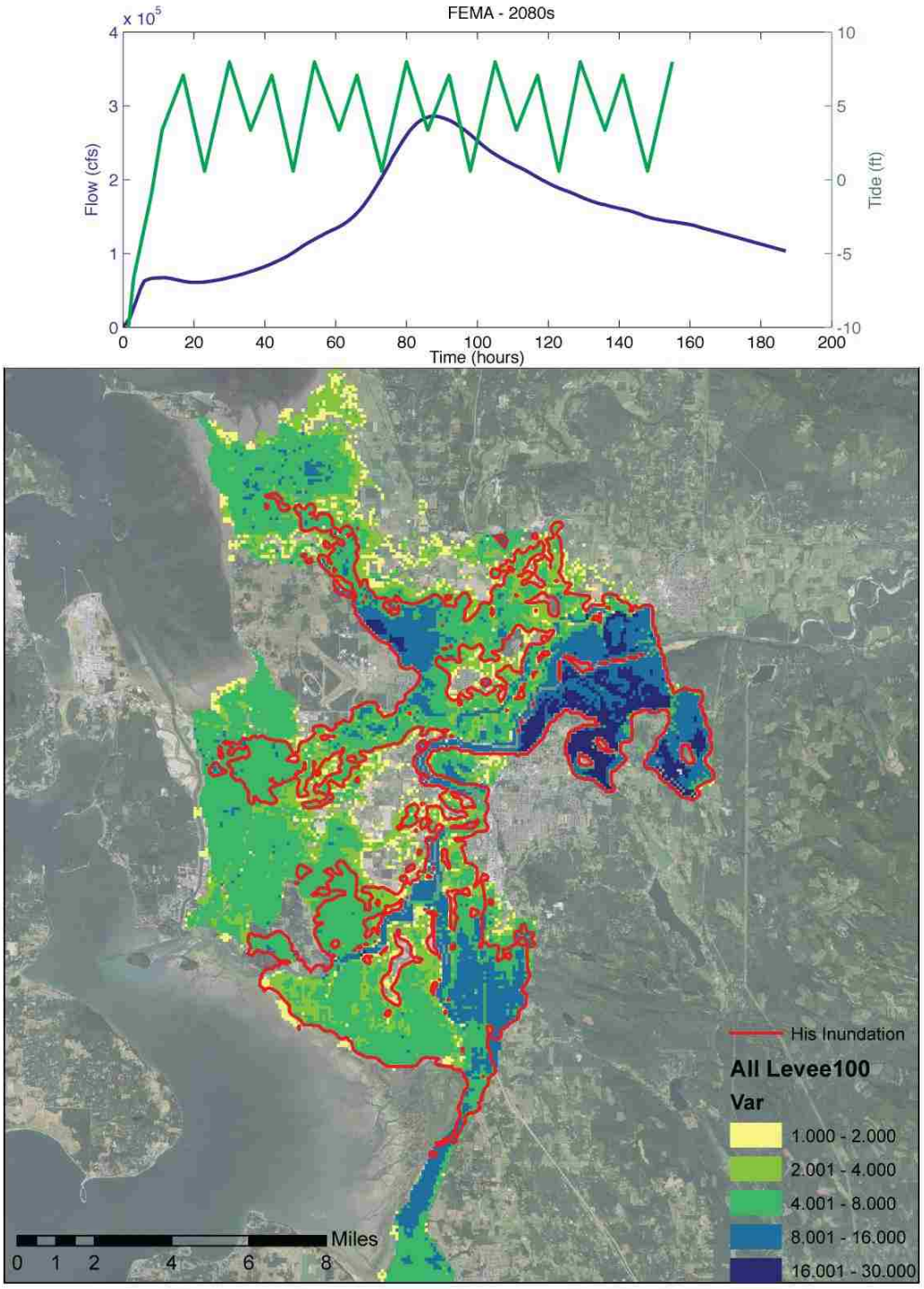

Figure 24 – 2080s scaled FEMA 100-yr inundation map for the "No Levee Failure" Scenario in the Skagit River Basin. Red lines represent the historical FEMA 100-yr flood inundation. The top panel represents the inflow and outflow boundary conditions. Units: Feet.

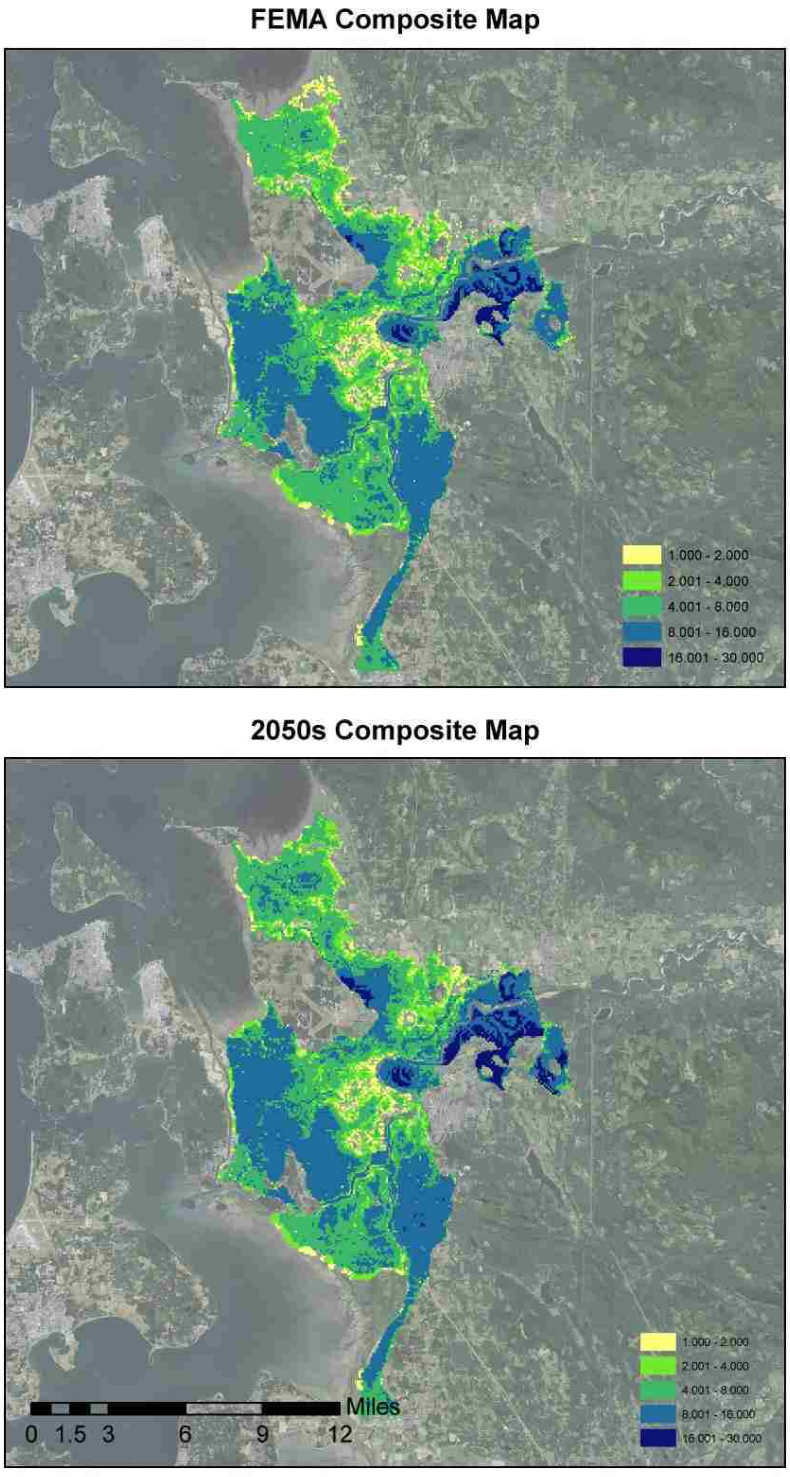

Figure 25- Composite inundation maps using 7 levee failure scenarios. A) FEMA event, B) Scaled 2050s FEMA event. Units: Feet.

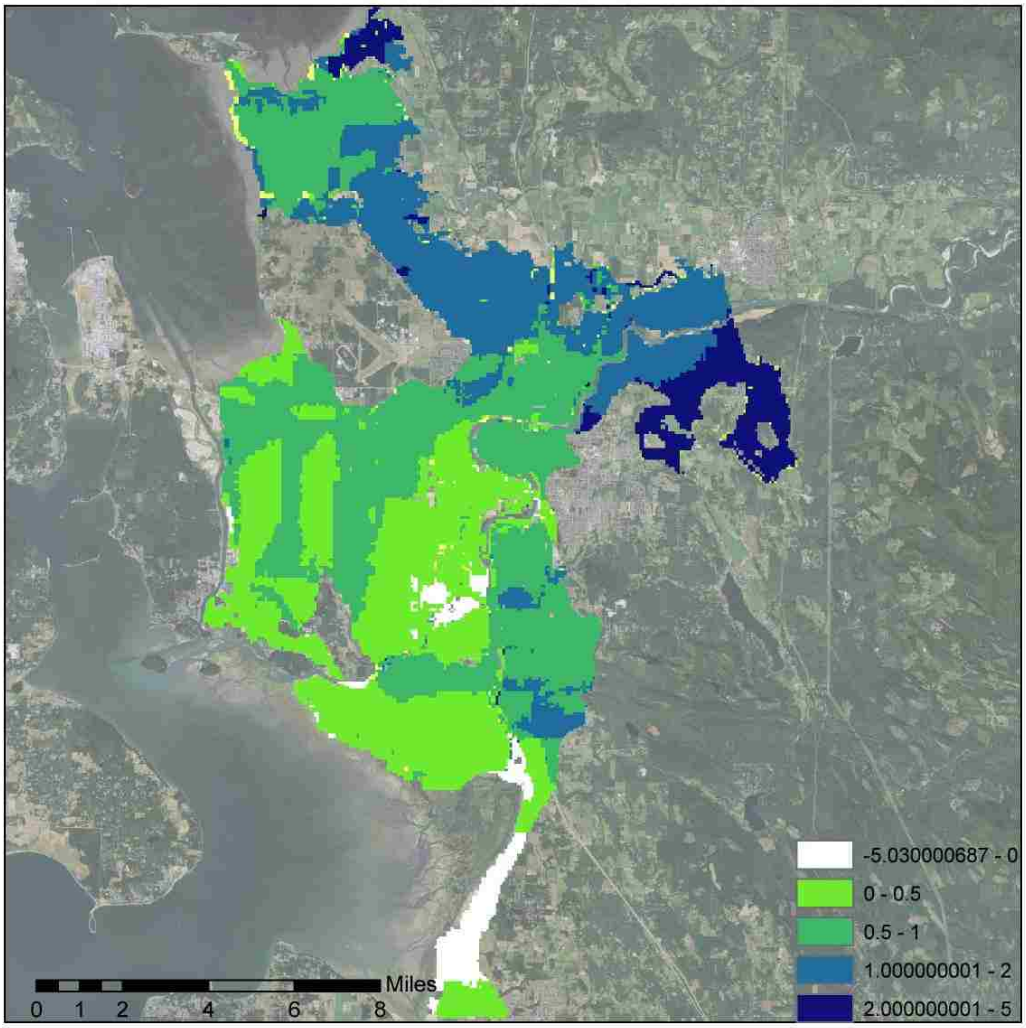

Figure 26 - Difference between FEMA composite inundation map (25A) and 2050s composite inundation map (25B). Units: Feet.

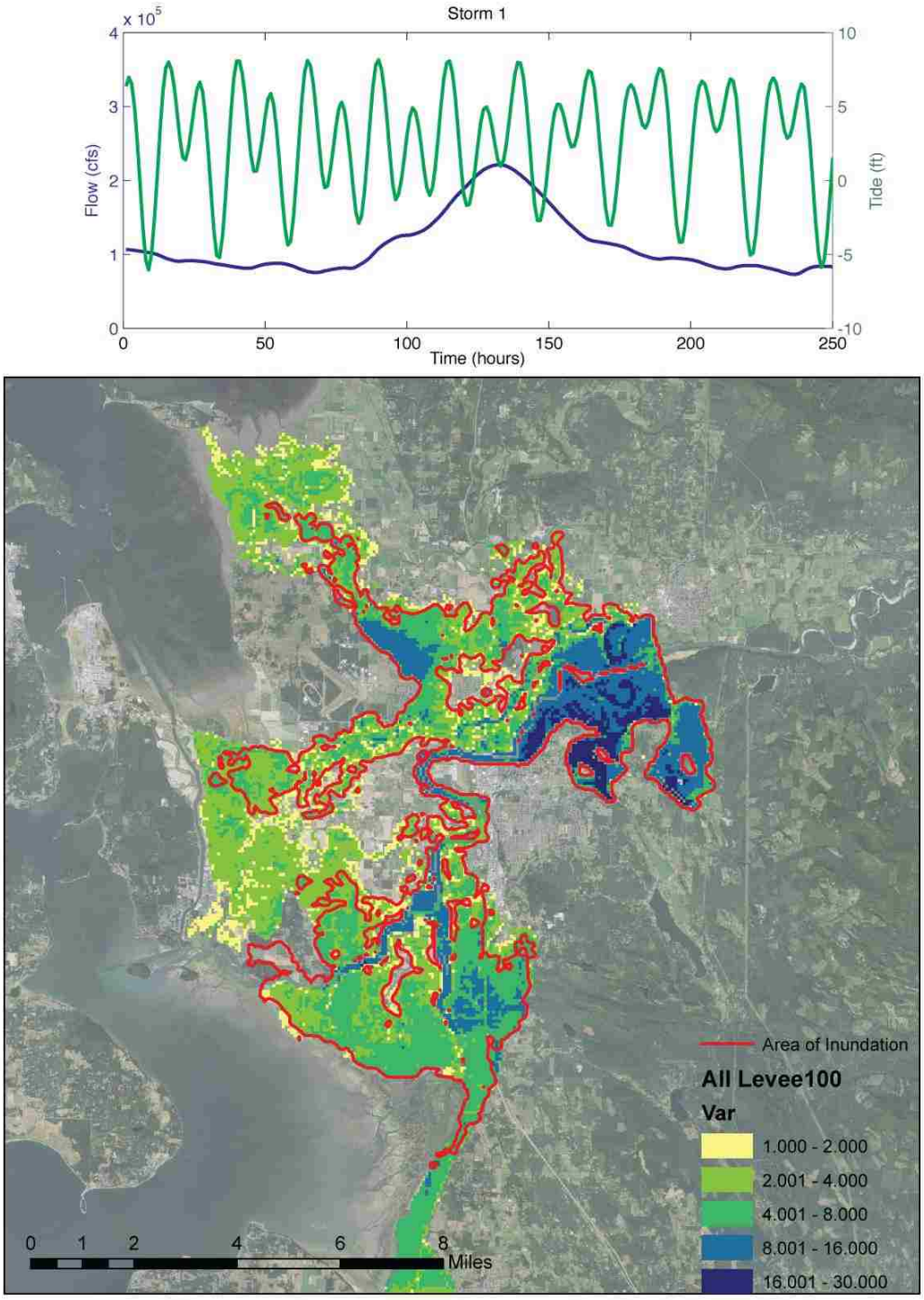

Figure 27 – Storm 1 – WRF-2050s inundation map for the "No Levee Failure" Scenario in the Skagit River Basin. Red lines represent the historical FEMA 100-yr flood inundation. The top panel represents the inflow and outflow boundary conditions. Units: Feet.

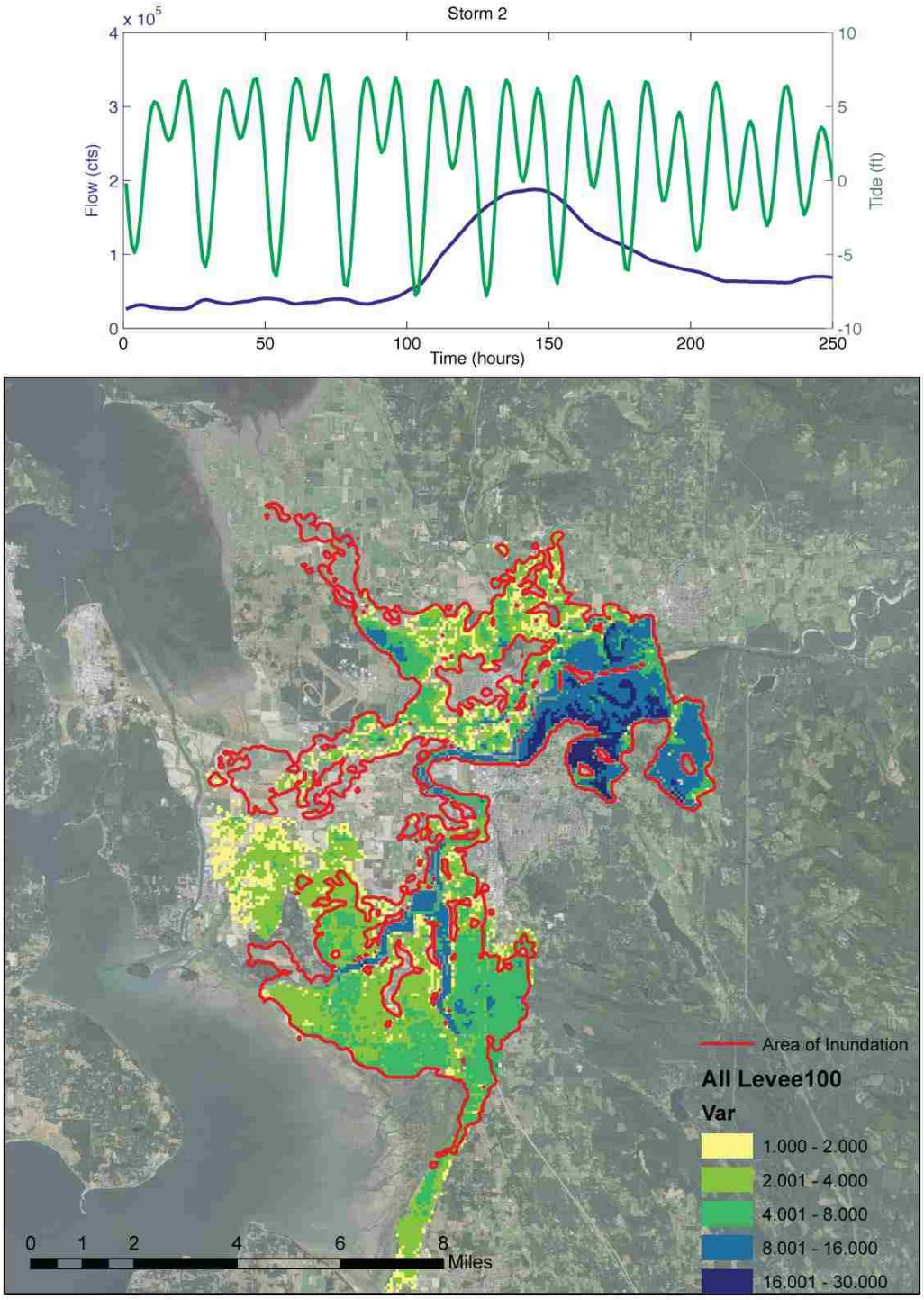

Figure 28 - Storm 2 – WRF-2050s inundation map for the "No Levee Failure" Scenario in the Skagit River Basin. Red lines represent the historical FEMA 100-yr flood inundation. The top panel represents the inflow and outflow boundary conditions. Units: Feet.

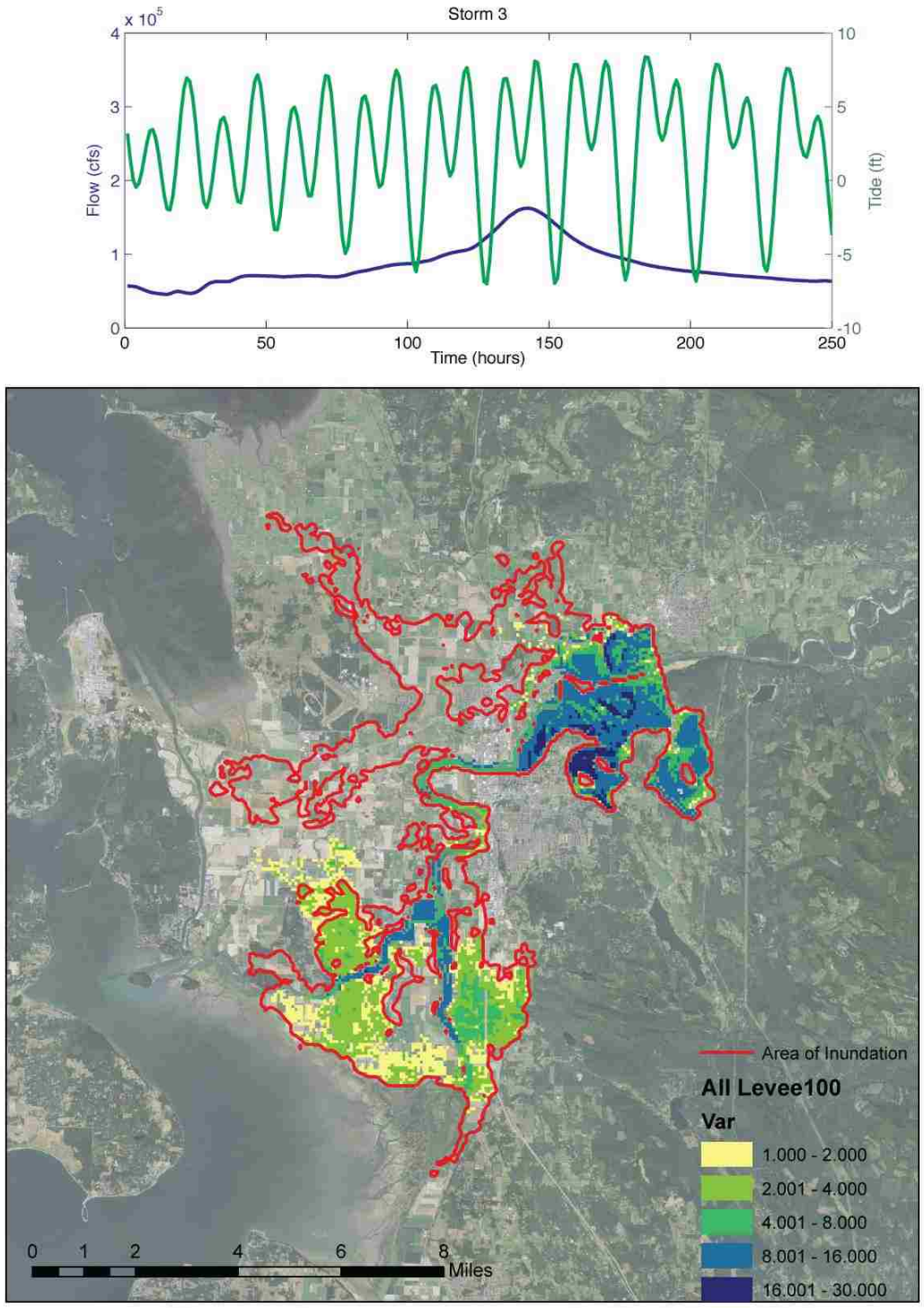

Figure 29 - Storm 3 – WRF-2050s inundation map for the "No Levee Failure" Scenario in the Skagit River Basin. Red lines represent the historical FEMA 100-yr flood inundation. The top panel represents the inflow and outflow boundary conditions. Units: Feet.

5 Conclusions

As we move further into the twenty-first century, global climate change is expected to significantly alter the climate of the PNW. Extreme high water levels in floodplains and estuaries in the Puget Sound lowlands are expected to be impacted by climate change via sea level rise and increased river flooding. The findings of this study further emphasize the inappropriate assumption of stationarity in flood plain management applications. This study uses dynamic and flexible approaches to establish future flood risk by modeling flood risk as it varies in time, a crucial adjustment that needs to be made by the floodplain management community.

Sediment and species distribution is dependent on large flood events. While the formation of deltas is fundamentally linked to the sediment transport regimes in rivers, the survival of deltaic ecosystems are closely tied to the estuarine water levels. If water levels are too high, many portions of these ecosystems can drown; if water levels are too low, deltas are starved of nutrient rich sediment and water. Sea level rise and increased river flooding threaten to disturb the balance of these systems.

Increases in the 10-year unregulated peak annual flows in the Skagit and Nisqually Rivers are expected to exceed 25% by mid-century. These changes are consistent between downscaling techniques and are in line with the results of other studies. These increases are influenced both by warmer basin temperatures, which raise freezing lines and enlarge effective basin area, and increasing storm intensity.

A regression approach used to calculate storm surge yielded similar future and historical probability distributions. This minimal change in expected storm surges

reflects the consistent nature of future storm events in the regional climate model. Sea level rise, by comparison, is expected to play a much larger role in future Puget Sound tidal anomalies than changes in storm surge behavior. This effectively doubles the historic 100-yr storm surge by 2050. These increases will have substantial impacts on low lying Puget Sound areas, especially during large tidal events.

Estuarine water levels and inundated area in the Skagit River floodplain are shown to increase primarily due to the combined effects of sea level rise and increased regulated flood magnitudes. Flood inundation in the largest events is expected to increase by up to 80% by the 2050s in comparison to the present-day 100-yr event published by FEMA and the USACE in their recent Flood Insurance Study. A 2050s scaled version of the FEMA composite flood map shows average increases in flood depth of more than 10-inches across the lower Skagit River basin. The contrast between the present day 100-yr flood event used in this study and the projected future events highlights the need for alternative flood plain management strategies to cope with potentially much higher risks.

The new approaches developed in this study are intended to help provide a well-defined “road map” for future studies addressing the combined effects of future sea level rise, storm surge, and river flooding on extreme high water levels in coastal areas. Further evaluation of the application of regional climate models in studies such as these is needed to understand their effectiveness in resolving local scale climate and global teleconnections (i.e. ENSO, PDO, etc.). For this reason, increased realizations of regional scale climate models will be needed to better characterize the changing risks in the Puget Sound lowlands.

References

1. Bjornsson, H. & Venegas, S. A., 2007. *A Manual for EOF and SVD analyses of Climatic Data,* s.l.: Department of Atmospheric and Oceanic Sciences and Center for Climate and Global Change Research McGill University.
2. Bretherton, C. S., Smith, C. & Wallace, J. M., 1992. An Intercomparison of Methods for Finding Coupled Patterns in Climate Data. *Journal of Climate,* pp. 541-560.
3. Brown, D. P. & Comrie, A. C., 2004. A winter precipitation 'dipole' in the western United States associated with multidecadal ENSO variability. *Geophysical Research Letters,* pp. 1-4.
4. Cayan, D. R. et al., 2008. Climate change projections of sea level extremes along the California coast. *Climate Change,* pp. S57-S73.
5. Cayan, D. R. et al., 2001. Changes in the Onset of Spring in the Western United States. *Bulletin of the American Meteorological Society,* pp. 399-415.
6. Church, J. A. & White, N. J., 2006. A 20th century acceleration in global sea-level rise. *Geophysical Research Letters,* pp. 1-4.
7. Church, J. A. et al., 2004. Estimates of the Regional Distribution of Sea Level Rise over the 1950-2000 Period. *Journal of Climate,* pp. 2609-2625.
8. Cunnane, C., 1978. Unbiased Plotting Positions - A Review. *Jourlnal of Hydrology,* pp. 205-222.
9. Duliere, V., Zhang, Y. & Salathe, E. P. J., 2011. Changes in 20th century extreme temperature and precipitation over the western United States from observations and regional climate model simulations. *Journal of Climate,* pp. 1950-1964.

10. Elsner, M. M. et al., 2010. Implications of 21st century climate change for the hydrology of Washington State. *Climatic Change,* pp. 225-260.

11. Federal Emergency Management Agency, TBD. *Flood Insurance Study, Skagit County, Washington,* s.l.: s.n.

12. Gao, H. et al., 2010. Water Budget Record from Variable Infiltration Capacity (VIC) Model. *Algorithm Theoretical Basis Document for Terrestrial Water Cycle Data Records.*

13. Goodrich, G. B., 2007. Influence of the Pacific Decal Oscillation on Winter Precipitation and Drought during Years of Neutral ENSO in the Western United States. *Weather and Forecasting,* pp. 116-124.

14. Hamlet, A., 1996. *Generating Basinwide Alternatives for the Apalachicola-Chattahoochee-Flint River Basin Using a Monthly-Time-Step, Hydrologic Screening Model, Master's Thesis, Department of Civil and Environmental Engineering, University of Washington, March,* s.l.: s.n.

15. Hamlet, A. et al., 2012. An Overview of the Columbia Basin Climate Change Scenarios Project: Approach, Methods, and Summary of Key Results. *Atmosphere-Ocean,* Volume (In Review).

16. Hamlet, A. F. et al., 2010. *Final Report for the Columbia Basin Climate Change Scenarios Project,* s.l.: s.n.

17. Hamlet, A. F. & Lettenmaier, D. P., 2005. Production of Temporally Consistent Gridded Precipitation and Temperature Fields for the Continental United States. *Journal of Hydrometeorology,* pp. 330-336.

18. Hamlet, A. F. & Lettenmaier, D. P., 2007. Effects of 20th century warming and climate variability on flood risk in the western U.S.. *Water Resources Research,* Volume 43, pp. 1-17.

19. Hamlet, A. F., Mote, P. W., Clark, M. P. & Lettenmaier, D. P., 2005. Effects of Temperature and Precipitation Variability on Snowpack Trends in the Western United States. *Journal of Climate,* pp. 4545-4561.

20. Hamlet, A. & Lettenmaier, D., 1999. Effects of climate change on hydrology and water resources in the Columbia River basin. *Journal of American Water Resources Association,* 25(6), pp. 1597-1623.

21. IPCC, 2007. *Climate Change 2007: The physical Science Basis, Contribution of Working Group I to the Fourth Assessment Report of the Intergovernmental Panel on Climate Change, S.Solomon et al.,* Cambridge: Cambridge University Press.

22. ISEE, 2012. *STELLA Modeling and Simulation Software.* [Online] Available at: http://www.iseesystems.com/softwares/Education/StellaSoftware.aspx [Accessed 1 5 2012].

23. Lee, S.-Y. & Hamlet, A., 2011. *Skagit River Basin Climate Science Report, a summary report prepared for Skagit County and the Envision Skagit Project by the Department of Civil and Environmental Engineering and The Climate Impacts Group at the University of Washington,* s.l.: s.n.

24. Lee, S.-Y., Hamlet, A. F., Fitzgerald, C. J. & Burges, S. J., 2009. Optimized Flood Control in the Columbia River Basin for Global Warming Scenario. *Journal of Water Resources Planning and Management,* pp. 440-450.

25. Liang, X., Lettemaier, D., Wood, E. & Burges, S., 1994. A simple hydrologically based model of land surface water and energy fluxes for GSMs. *Journal of Geophysical Research,* 99(14), pp. 415-428.

26. Liang, X., Wood, E. & Lettenmaier, D., 1996. Surface soil moisture parameterization of the VIC-2L model: Evaluation and modifications.. *Global Planet Change,* Volume 13, pp. 195-206.

27. Lin, J.-L., 2007. Interdecadal variability of ENSO in 21 IPCC AR4 coupled GCMs. *Geophysical Research Letters,* Volume 34, pp. 1-6.

28. Littell, J. S., McKenzie, D., Peterson, D. L. & Westerling, A. L., 2009. Climate and wildfire area burned in western U.S. ecoprovinces, 1916-2003. *Ecological Applications,* 19(4), pp. 1003-1021.

29. Loganathan, G., Kuo, C. & Yannaccone, J., 1987. Joint Probability Distribution of Streamflows and Tides in Estuaries. *Nordic Hydrology,* Volume 18, pp. 237-246.

30. Mantua, N. J. & Hare, S. R., 2002. The Pacific Decadal Oscillation. *Journal of Oceanography,* pp. 35-44.

31. Mantua, N. J. et al., 1997. A Pacific Interdecadal Climate Oscillation with Impacts on Salmon Production. *Bulletin of the American Meteorological Society,* pp. 1069-1079.

32. Mantua, N., Tohver, I. & Hamlet, A., 2010. Climate change impacts on streamflow extremes and summertime stream temperature and their possible consequences for freshwater salmon habitat in Washington State. *Climatic Change,* pp. 187-223.

33. Mass, C. F. et al., 2003. Regional Environmental Prediction over the Pacific Northwest. *American Meteorological Society,* pp. 1353-1366.

34. McKenzie, D., Gedalof, Z., Peterson, D. & Mote, P., 2004. Climatic Change, wildfire, and conservation. *Conserv Biol,* 18(4), pp. 890-902.

35. Milly, P. C. D. et al., 2008. Stationarity Is Dead: Whither Water Management?. *Science,* pp. 573-574.

36. Mote, P., Hamlet, A., Clark, M. & Lettenemier, D., 2005. Declining Mountain Snowpack in Western North America. *Bulletin of the American Meteorological Society,* Volume 86, pp. 39-49.

37. Mote, P. et al., 2008. *Sea Level Rise in the Coastal Waters of Washington State,* s.l.: University of Washington Climate Impacts Group.

38. Mote, P. W., 2003. Trends in Temperature and Precipitation in the Pacific Northwest During the Twentieth Century. *Northwest Science,* pp. 271-282.

39. Mote, P. W. & Salathe, E. P., 2010. Future climate in the Pacific Northwest. *Climatic Change,* Volume 102, pp. 29-50.

40. Nicholls, R. J. & Cazenave, A., 2010. Sea-Level Rise and Its Impact on Coastal Zones. *Science,* pp. 1517-1520.

41. Nijssen, B. et al., 1997. Streamflow simulation for continental-scale river basins.. *Water Resources Research,* Volume 33, pp. 711-724.

42. R. Pawlowicz, B. B. a. S. L., 2002. Classical tidal harmonic analysis including error estimates in MATLAB using T_TIDE. *Computers and Geosciences,* pp. 929-937.

43. Salathé , E. P., Mote, P. W. & Wiley, M. W., 2007. Review of scenario selection and downscaling methods for the assessment of climate change impacts on hydrology in the United States pacific Northwest. *International Journal of Climatology,* pp. 1611-1621.

44. Salathe, E. P. et al., 2012. Estimates of 21st Century Flood Risk in the Pacific Northwest Based on Regional Scale Climate Model Simulations. *In review,* pp. 1-26.

45. Salathe, E. P. J., Leung, L. R., Qian, Y. & Yongzin, Z., 2010. Regional climate model projections for the State of Washington. *Climatic Change,* pp. 51-75.

46. Smith, T. M., Reynolds, R. W., Peterson, T. C. & Lawrimore, J., 2008. Improvements to NOAA's Historical Merged Land-Ocean Surface Temperature Analysis. *Journal of Climate,* pp. 2283-2296.

47. Stammer, D. & Huttemann, S., 2008. Response of Regional Sea Level to Atmospheric Pressure Loading in Climate Change Scenario. *Journal of Climate,* pp. 2093-2010.

48. Stewart, I. T., Cayan, D. R. & Dettinger, M. D., 2005. Changes toward Earlier Streamflow Timing across Western North America. *Journal of Climate,* Volume 18, pp. 1136-1155.

49. Tan, K.-S., Chiew, F. H. S. & Grayson, R. B., 2007. A steepness index unit volume flood hydrograph approach for sub-daily flow disaggregation. *Hydrological Processes,* Volume 21.

50. Tebaldi, C., Strauss, B. H. & Zervas, C. E., 2012. Modelling sea level rise impacts on storm surges along US coasts. *Environmental Research Letters,* pp. 1-11.

51. Trenberth, K., 1997. The definition of El Nino.. *Bulliten of American Meteorological Society,* Volume 71, pp. 988-993.

52. Trenberth, K. et al., 2007. *Observations: Surface and Atmospheric Climate Change. In: Climate Change 2007: The Physical Science Basis. Contribution of Working Group I to the Fourth Assessment Report of the Intergovernmental Panel on Climate Change,* Cambridge, United Kingdom and New York, NY, USA: Cambridge University Press.

53. U.S. Army Corps of Engineers, 2007. *Skagit River Basin, Washington, Revised Flood Insurance Study, Draft Hydaulics Summary,* Seattle: Seattle District.

54. U.S. Army Corps of Engineers, 2008. *Draft, Skagit River Basin, Washington, Revised Flood Insurance Study, Hydrology Study,* Seattle: Seattle District.

55. U.S. Army Corps of Engineers, 2009. *Skagit River Basin, Washington, Revised Flood Insurance Study, Hydaulics Summary,* Seattle: Seattle District.

56. University of Washington, Climate Impacts Group, n.d. *http://cses.washington.edu/cig/pnwc/clvariability.shtml.* [Online] Available at: http://cses.washington.edu/cig/pnwc/clvariability.shtml [Accessed 29 5 2012].

57. Vano, J. A. et al., 2010. *Climate change impacts on water management and irrigated agriculture in the Yakima River Basin, Washington, USA,* 2010: Climatic Change.

58. Vermeer, M. & Rahmstorf, S., 2009. Global sea level linked to global temperature. *PNAS,* pp. 1-6.

59. von Storch, H. & Navarra, A., 1995. *Analysis of Climate Variability.* Berlin: Pringer-Verlag Berlin Heidelber.

60. Wallace, J. M., Smith, C. & Bretherton, C. S., 1992. Singular Value Decomposition of Wintertime Sea Surface Temperature and 500-mb Height Anomalies. *Journal of Climate,* pp. 561-576.

61. Wang, H., Tang, M. & Ji, M., 1999. Prediction of seasonal mean United States precipitation based on El Nino sea surface temperatures. *Geophysical Research Letters,* pp. 1341-1344.

62. Wood, A. W., Maurer, E. P., Kumar, A. & Lettenmaier, D. P., 2002. Long range experimental hydrologic forecasting for the Eastern U.S.. *Journal of Geophysical Research,* Volume 107.

Appendix A: Singular Value Decomposition

Spatial and coupled climate patterns are often difficult to distinguish from one another due to their overlapping nature. Singular value decomposition (SVD) is a mathematical technique that produces discrete modal representations of the spatial patterns and the corresponding temporal signals describing the observed variance. This technique is similar to empirical orthogonal function analysis and principal component analysis. Methods such as the SVD have been widely used in studies examining the nature of complicated large scale coupled climate patterns (Bretherton, et al., 1992; Wallace, et al., 1992; von Storch & Novarra, 1995). The process of deriving the principal component time series from gridded pressure anomalies follows the direction of Bjornsson & Venegas (2007) and is outlined below.

Gridded daily surface pressure anomalies from the WRF-Reanalysis and WRF-ECHAM-5 runs were regrided from 1/8° × 1/8° to approximately 1/4° × 1/4° for computational purposes. These anomalies were then reshaped such that each timestep was represented by a single matrix row.

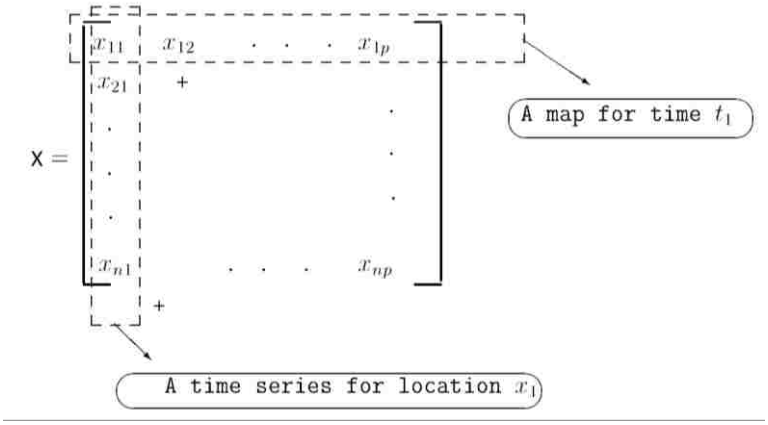

Figure A1 – Matrix Structure used for the SVD analysis.

The SVD computations were performed using MATLAB preloaded functions. The SVD function is shown as $[U, S, V] = svd(X)$. This function produces three matrices, whose product represent the closest k = rank(x) approximation of X. The U matrix represents the principle components, the S, or Σ, matrix represents the singular values, and the V* matrix effectively eigenvectors for each mode (Figure A2).

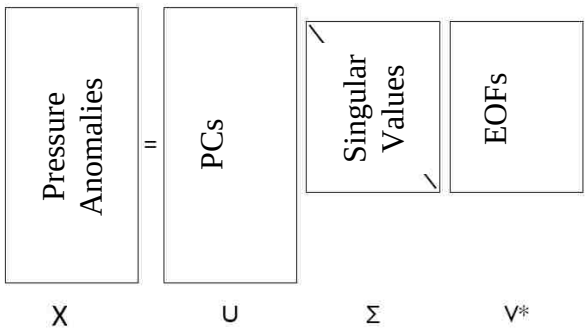

Figure A2 - Input (X) and output (U, S, and V) for the singular value decomposition.

The principal components from the WRF-Reanalysis were used as training inputs into the storm surge regression model described in section 3.6. In this way, the spatial structure defined by the leading EOFs is explicitly included in the regression model. To insure that the same spatial structure is used as inputs into the regression model, the pressure fields associated with the future run (WRF-ECHAM-5 1970-2069) were projected directly onto spatial EOFs from the WRF-Reanalysis. By inverting the decomposition process, the spatial EOFs and their relative weight can be held constant while new inputs (X') represent the gridded pressure anomalies. The result is U', which represents the principal component time series for the future pressure fields.

$$U' = v * s \backslash X'$$

Appendix B: ENSO Calculation

There are a number of different techniques designed to quantify the behavior of the El Niño Southern Oscillation (ENSO). The teleconnection between ENSO and North American climate variability has been widely acknowledged (Wallace, et al., 1992; Mantua, et al., 1997; Wang, et al., 1999; Brown & Comrie, 2004; Goodrich, 2007). In the Pacific Northwest, the warm phase of the oscillation (El Niño) is often accompanied by warmer and drier winters, whereas the cool phase (La Niña) is often accompanied by cooler and wetter winters. This relationship has been shown to influence peak annual floods (Hamlet & Lettenmaier, 2007). Figure 9A also shows a linear relationship between ENSO and regional sea level.

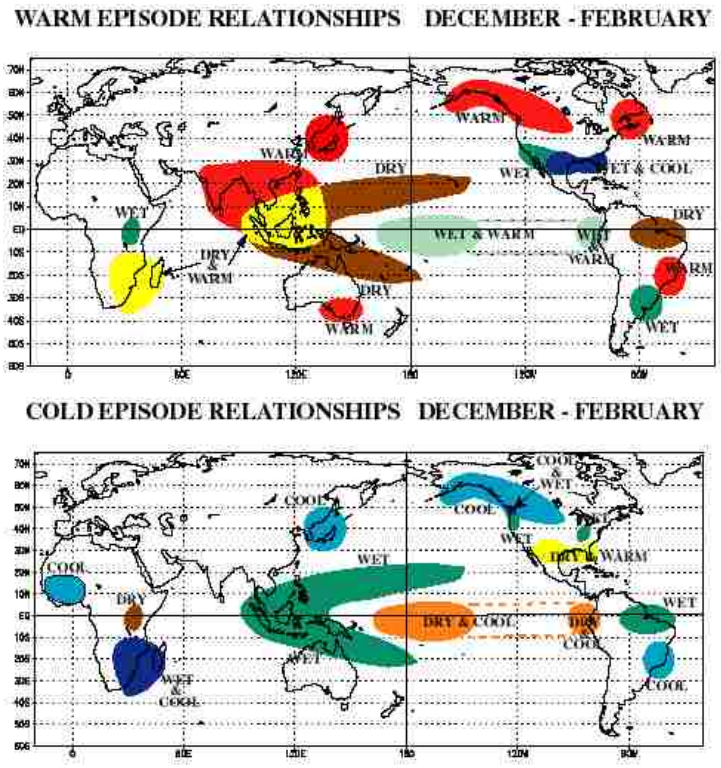

Figure B1 – Global teleconnections of El Niño Southern Oscillation. A) Warm Episode (El Niño), B) Cold Episode (La Nina) during winter season. In the Pacific Northwest El Niño is associated with warm winter temperatures while the La Niño is associated with cold and wet winter conditions. Source: NOAA Climate Prediction Center.

Originally quantified as the difference in monthly surface pressure between Tahiti and Darwin, Australia; later studies found that the interannual variability of westerly winds and SSTs is better described by the areal averaged sea surface temperature anomalies in the equatorial Pacific. Recently, the Niño3.4 index has become the most popular method to describe the oscillation. The Niño3.4 is defined as the 5-month running mean of sea surface temperature anomalies in the region, 5°N-5°S, 120°-170°W (Trenberth, 1997). The extraction of the Niño3.4 index from the coupled ECHAM-5/ MPI-OM model results followed the following steps. Figure 9B shows the time series of the observed and GCM derived Niño3.4 index.

1. Analyze monthly mean SSTs in 2° × 2° grids.
2. Calculate monthly SST anomalies averaged for the area 5°N-5°S, 120°-170°W.
3. Find 5-month running mean of averaged SST anomalies.

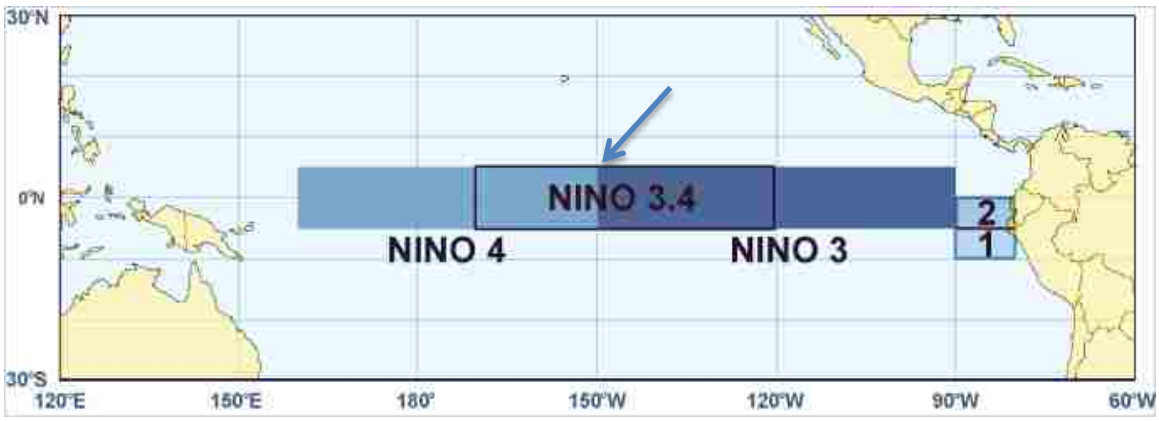

Figure B2 - The Niño3.4 region is defined as the area between 5°N-5°S, 120°-170°W.

Appendix C: Floodplain Mapping

The floodplain mapping performed for this study was modeled after the methods used by the USACE and FEMA in the recent studies performed in the Skagit River Basin (USACE, 2007; USACE, 2008; USACE, 2009; FEMA, TBD). In this group of studies, the Skagit River Flo2D model was developed and calibrated. The flood protection situation in lower Skagit River is unique because, although levees line much of the river, the levees do not provide protection against large flood events. Additionally, the levees in the Skagit Basin have repeatedly failed during large flood events creating local extreme flooding. To capture the behavior of flooding under different levee failure scenarios, USACE and FEMA performed separate modeling exercises for 7 levee scenarios:

1. All Levees Intact
2. Left Bank Levees Removed
3. Fir Island Levees Removed
4. South Fork Right Bank Levee Removed
5. North Fork Left Bank Levee Removed
6. Right Bank Levees Removed Except South Fork
7. Left Bank Levees Removed Except North Fork

For each scenario, the flow depths were extracted based on the areas shown in figure C1. Composite maps were constructed by combining the flow depths for each scenario area (figure 22). Because of the unpredictable nature of levee failures, these maps are meant to depict a “worst case scenario” for each area within the basin.

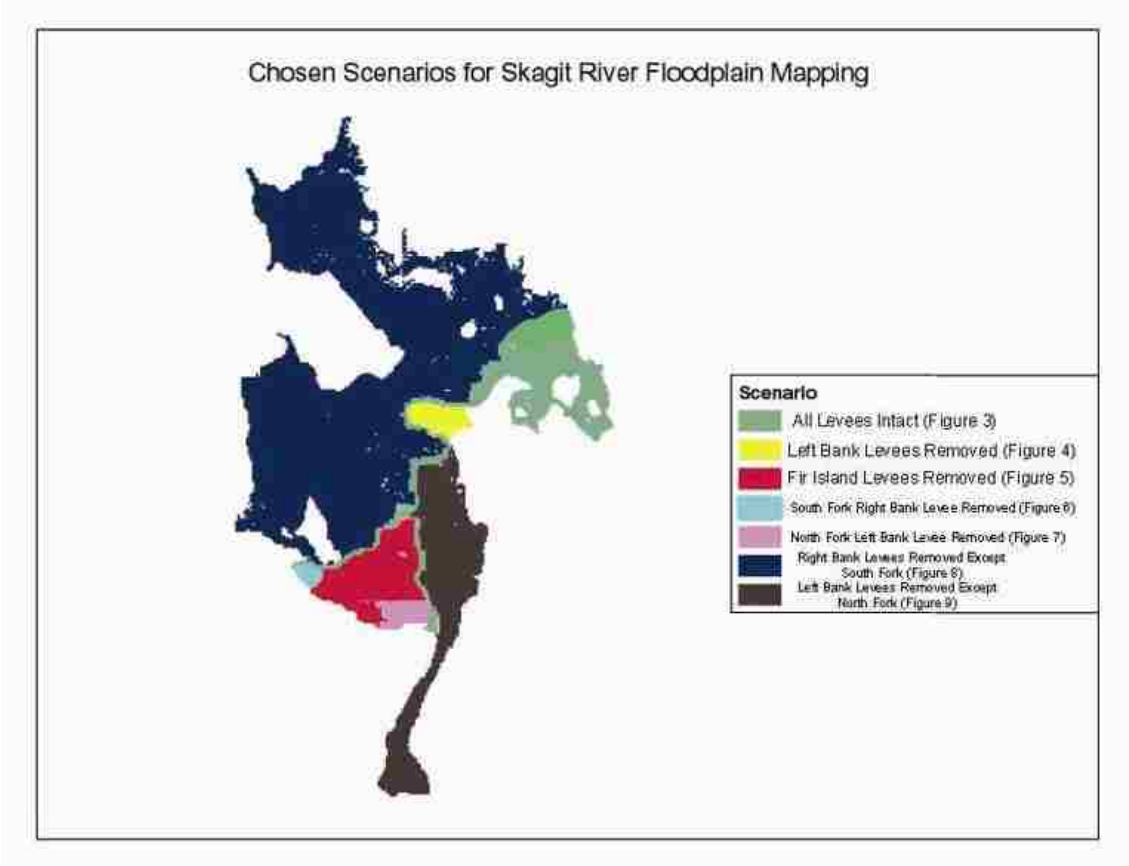

Figure C1 – Levee scenarios in the Skagit River Basin. The flow depths for each scenario are extracted based on this figure. The seven scenarios are then combined to form a composite flow depth map.

Comparing the spatial extent of figures 22 and C1, it should be acknowledged that nearly every cell in model domain is flooded in both the FEMA and 2050s model runs. Although it was beyond the scope of this project, expanding the extent of the model domain might provide different results, especially near the horizontal boundaries. Similarly, the largest flood depths were simulated in the upper portions of the basin near the upstream boundary. Expanding the model domain upstream would allow for better resolution of flood dynamics in this area.

Lastly, the results from the sensitivity analysis are shown in figure 27. Evaluating the FEMA hydrograph with projected 2050s SLR, inundated area increases from 42,266 acres to 57,043 acres. Larger increases are found when the 2050s scaled FEMA 100-yr

flood is modeled without sea level rise. In this case, inundated area is approximately equal to the combined SLR/increased flooding amount. This is likely because the size of the flood is so great that most of the near shore floodplain is flooded based on the flow volume alone.